

1 **Temperature decomposition of paired site observations reveals new insights**  
2 **in climate models' capability to simulate the impact of LUC.**

3

4 **Sam Vanden Broucke<sup>1</sup>, Sebastiaan Luyssaert<sup>2</sup>, Edouard Davin<sup>3</sup>, Ivan Janssens<sup>4</sup> & Nicole**  
5 **van Lipzig<sup>1</sup>**

6

7 [1] Department of Earth and Environmental Sciences, University of Leuven, Belgium

8 [2] Le Laboratoire des Sciences du Climat et de l'Environnement (LSCE), France

9 [3] Institute for Atmospheric and Climate Science, ETH Zürich, Switzerland

10 [4] Plant and Vegetation Ecology, University of Antwerp, Belgium

11

12 Corresponding author: Sam Vanden Broucke (sam.vandenbroucke@ees.kuleuven.be)

13 University of Leuven

14 Department of Earth and Environmental Sciences

15 Celestijnenlaan 200E

16 B – 3001 Leuven

17

## 18 **Key Points**

- 19 • A new methodology for evaluating the biogeophysical climate impact of LUC in  
20 climate models is presented.
- 21 • This methodology is applied to a state of the art regional climate model.
- 22 • The main model biases in simulating observed LUC related mechanisms are  
23 identified.

## 24 **Abstract**

25 In this study, we present a new methodology for evaluating the biogeophysical impact of land  
26 use change (LUC) in climate models. For this, we use observational data from paired eddy  
27 covariance flux towers in Europe, representing a LUC from forest to open land  
28 (deforestation). Two model simulations with a regional climate model (COSMO-CLM<sup>2</sup>) are  
29 performed which differ only in prescribed land use for site pair locations. The model is  
30 evaluated by comparing the observed and simulated difference in surface temperature (Ts)  
31 between open land and forests. Next, we identify the biogeophysical mechanisms responsible  
32 for Ts differences by applying a Ts decomposition method to both observations and model  
33 simulations, allowing us us to determine which LUC related mechanisms were well  
34 represented in COSMO-CLM<sup>2</sup>, and which were not. Results show that deforestation leads to a  
35 significant cooling at night, which is severely underestimated by COSMO-CLM<sup>2</sup>. It appears  
36 the model is missing one crucial impact of deforestation on the nighttime surface energy  
37 budget: a reduction in downwelling longwave radiation. Results are better for daytime, as the  
38 model is able to simulate the increase in albedo and associated surface cooling following  
39 deforestation reasonably well. Also well simulated, albeit underestimated slightly, is the  
40 overall decrease in sensible heat flux caused by reduced surface roughness. Overall, these  
41 results stress the importance of differentiating between daytime and nighttime climate when  
42 discussing the effect of LUC on climate. Finally, we believe they provide new insights  
43 supporting a wider application of the methodology (to other regional climate models).

44

45

## 46 **Keywords**

47 Land-atmosphere interactions, land-use change, deforestation, model evaluation

48

## 49 1 Introduction

50 Research has shown that land use change (LUC) can have a significant biogeophysical impact  
51 on climate in the regions in which it occurs [*Bonan, 2008; Bala et al., 2007; Davin and de*  
52 *Noblet-Ducoudré, 2010; Mahmood et al., 2014*], and if large enough, may cause global effects  
53 [*Werth and Avissar, 2002; Werth and Avissar, 2005; Hasler et al., 2009; Medvigy et al.,*  
54 *2013*]. It is therefore essential that the biogeophysical impact of LUC is modeled correctly in  
55 climate models. Currently, modelers rely mostly on standalone usage of land surface models  
56 (LSM's) to evaluate performance over different land use types (e.g. [*Viterbo and Beljaars,*  
57 *1995; van den Hurk et al., 2000; Krinner et al., 2005; Abramowitz et al., 2008; Lauwaet et al.,*  
58 *2008; Stöckli et al., 2008; Akkermans et al., 2012; Demuzere et al., 2013*]). In standalone or  
59 so-called offline runs, the LSM is uncoupled from the climate model's atmospheric  
60 component and is instead driven by local measured atmospheric conditions (e.g. incoming  
61 shortwave and longwave radiation, atmospheric temperature and humidity, etc.) in single  
62 grid-cell mode. Model performance is then evaluated by comparing the LSM's response to  
63 this prescribed atmosphere (sensible heat flux, latent heat flux, bowen ratio, soil moisture,  
64 etc.) to the measured response. This exercise is usually repeated for a series of different land  
65 use types.

66 Although this method of evaluating is useful and necessary, it does not, by itself, represent a  
67 complete evaluation of LUC effects in climate models. First, the model's ability to simulate  
68 the impact of a transition in land use is not evaluated directly. Rather, it is implicitly assumed  
69 that if the LSM simulates the surface climatology of two distinct land use types adequately, it  
70 is able to simulate the impact of a transition in land use between these two types as well.  
71 However, acceptable model biases in the surface climatology for two land use types could still  
72 result in an unacceptably large bias in the modeled difference. Second, offline runs do not  
73 account for surface-atmosphere feedbacks, while model inter-comparison studies have shown  
74 that these indirect LUC effects are important drivers in various current generation climate  
75 models [*Boisier et al., 2012; Boisier et al., 2013*].

76 It is therefore important, in addition to offline LSM evaluation efforts, to evaluate the impact  
77 of LUC in coupled land-atmosphere climate models. The need for such evaluation is further  
78 underscored by a recent model inter-comparison project called LUCID (Project Land-Use and  
79 Climate, Identification of Robust Impacts) [*Pitman et al., 2009*]. In this project, seven climate  
80 models are used to simulate the biogeophysical impact of historic forest clearing (from  
81 preindustrial to present day times), using global simulations. Results for temperature are

82 relatively consistent, with all but one out of seven models simulating a cooling in the northern  
83 hemisphere. Furthermore, all seven models simulate a decrease in available energy due to  
84 increased albedo [*Boisier et al.*, 2012]. However, the climate models disagree substantially on  
85 how the surface responds to this energy deficit. Although all models simulate a decrease in  
86 the sum of turbulent fluxes, the amount varies. The decrease in turbulent fluxes is higher in  
87 magnitude than the increase in albedo for some models and lower for others [*de Noblet-*  
88 *Ducoudré et al.*, 2012]. Also, models disagree substantially on the partitioning of the decrease  
89 in turbulent fluxes over latent and sensible heat. For example, despite the decrease in  
90 available energy, three models simulate an increase in summer latent heat flux for the  
91 northern hemisphere, while the others simulate the opposite response [*Pitman et al.*, 2009].

92 Several aspects of the impact of LUC in coupled land-atmosphere climate models have  
93 recently been evaluated. For example, the changes in albedo (*Boisier et al.*, 2013) and  
94 evapotranspiration (ET) [*Boisier et al.*, 2014] modeled in the LUCID simulations were  
95 compared to reconstructed change maps by *Boisier et al.* For albedo, *Boisier et al.* [2013] were  
96 able to determine if the bias of individual ensemble members was due to a bias in the extent  
97 of simulated snow cover or due to a bias in how both snow surface albedo and vegetated  
98 surface albedo was parameterized. The parameterization was shown to be more important  
99 than the snow cover extent. For ET, the model ensemble was shown to underestimate the  
100 decrease since preindustrial times [*Boisier et al.*, 2014]. However, uncertainty on the  
101 reconstructed ET decrease was reported to be high, due in part to the uncertainty in the  
102 observational ET datasets, but also due to a large dependency on the adopted land-use map.  
103 Moreover, preindustrial ET values were derived using present day data for the environmental  
104 drivers (precipitation, radiation, etc.), so potential atmospheric feedbacks were not accounted  
105 for [*Boisier et al.*, 2014]. Also, it is worth noting that both of these evaluation studies focus on  
106 evaluating climate models using observational data for only one surface energy budget  
107 component at a time.

108 In addition, existing studies that evaluate the impact of LUC in coupled land-atmosphere  
109 climate models rarely distinguish between daytime and nighttime climate, instead limiting the  
110 analysis to daily means. However, large differences in physical properties exist between the  
111 convective and nocturnal planetary boundary layer. Therefore, it is likely that the response to  
112 LUC differs significantly between day and night. Furthermore, studies have detected a  
113 disproportionate nocturnal contribution to near surface warming in historic surface  
114 temperature records [*Karl et al.*, 1993; *Vose, Easterling, and Gleason*, 2005; *Nair et al.*,

115 2011]. Possible responsible factors include tropospheric aerosols, greenhouse gases and  
116 clouds. LUC has been proposed as a possible factor as well [Zhou *et al.*, 2007]. It is therefore  
117 worthwhile to investigate if LUC has an impact on nighttime climate, and whether that impact  
118 is to dampen or enhance recent warming. If done using modeling studies, this means that  
119 climate models should be evaluated specifically for their ability to model the nighttime impact  
120 of LUC.

121 In this study, we present a new method for evaluating a climate model's ability to simulate the  
122 impact of LUC which extends above mentioned studies to a simultaneous evaluation of the  
123 impact of LUC on all surface energy budget components in a coupled land-atmosphere  
124 climate model. Our methodology consists of (1) a direct evaluation of the differences in  
125 surface climate instead of evaluating land use types separately, (2) online model simulations  
126 which account for atmospheric feedbacks, (3) a separate analysis of daytime and nighttime  
127 climate, (4) a simultaneous evaluation of all surface energy budget components and (5) an  
128 evaluation of the models capacity to reproduce the underlying processes following a LUC.  
129 Next, we apply this new methodology to a state of the art regional climate model.

## 130 **2 Methods and materials**

### 131 **2.1 Observational data**

132 The term land use change incorporates many possible transitions. Examples are forest clearing  
133 for wood production and/or agricultural use, reforestation of former agricultural areas, the  
134 conversion of natural grasslands to irrigated agriculture and (sub)urbanization. To  
135 demonstrate the methods, we focus on the climate impact of deforestation over Europe and  
136 deforestation as the transition from forest to open land.

137 Instead of selecting individual sites representing a variety of land use types, which would be  
138 the starting point of a more typical evaluation, we selected sites where an open land flux  
139 tower and a forest tower are located in close proximity. When located sufficiently close to  
140 each other, one can assume these site pairs share the same background climate conditions and  
141 ideally even the same weather, for example, timing of particular events, occurrence of heat-  
142 waves, and extreme precipitation. Therefore, any differences in surface climate conditions  
143 between the two sites constituting a site pair (e.g. 2 meter air temperature, evapotranspiration,  
144 sensible heat flux) can be attributed to the difference in land use.

145 In order for observational sites to be selected, they have to 1) be located in the study domain,  
146 i.e., Europe, 2) consist of a forested site and an open land site which could be either a

147 cropland or a grassland, 3) be located less than 35 km apart from each other. The 35 km was  
148 chosen in accordance with the spatial resolution of the model (see section 2.2), 4) have a  
149 common measurement period of at least one year, and finally, 5) have at least measurements  
150 of 2m air temperature, net radiation, latent heat and sensible heat fluxes.

151 In total, 14 sites in the FLUXNET database match these criteria, and were subsequently  
152 combined in seven site pairs (Table 1 and Figure 1). The vegetation at the selected sites  
153 ranges from temperate, continental to subtropical-mediterranean, and contains diverse  
154 management regimes with the most common being yearly cutting for most of the meadows  
155 and occasional thinning at the forested sites. The forested sites include both deciduous and  
156 coniferous tree species.

157 The average linear distance between sites within a pair is 11.3 km; the average latitudinal  
158 distance between sites is 6.0 km. These values are in line with the average distances reported  
159 by other studies that use site pairs to study the impact of LUC [*Lee et al.*, 2011; *Baldocchi et*  
160 *al.*, 2013; *Luyssaert et al.*, 2014; *Zhang et al.*, 2014]. Elevation differences within a pair range  
161 from minor, i.e., the height difference between the site pairs in clusters DK1, DE1, CZ1, ES1  
162 and PT1 is limited to 100 m or less to relatively large, i.e., Collelongo is located almost 700  
163 meters higher than Amplero, which are the two sites which form site pair IT1.

## 164 **2.2 Models**

165 The regional climate simulations analyzed in this study are performed with the COSMO-  
166 CLM<sup>2</sup> model [*Davin et al.*, 2011; *Davin & Seneviratne*, 2012]. COSMO-CLM<sup>2</sup> couples the  
167 atmospheric component of the regional climate model COSMO-CLM (version 4.8) to the  
168 Community Land Model version 3.5 (CLM3.5), the land surface component of the  
169 Community Earth System Model (CESM). COSMO-CLM 4.8 thus differs from the standard  
170 COSMO-CLM by replacing the relatively simple land surface component included in the  
171 model with the more comprehensive CLM 3.5.

172 Model evaluations show that the standard version of COSMO-CLM 4.8 meets all  
173 requirements to qualify as a state of the art regional climate model [*Keuler, Radtke, and*  
174 *Georgievski*, 2012; *Kotlarski et al.*, 2014; *Vautard et al.*, 2013]. It has been used extensively  
175 over Europe for both regional climate modeling and numerical weather prediction [*Feldmann*  
176 *et al.*, 2013; *Lauwaet et al.*, 2013; *Baldauf et al.*, 2011], and has been applied to other major  
177 world regions as well [*Dosio et al.*, 2014; *Asharaf and Ahrens*, 2013; *Kothe, Lüthi, and*  
178 *Ahrens*, 2014; *Nikulin et al.*, 2012]. A recent model inter-comparison study performed for a

179 European model domain has shown that, compared to standard COSMO-CLM, COSMO-  
180 CLM<sup>2</sup> improves performance for several climate variables, including cloud cover, surface  
181 temperature and precipitation. The main factor explaining these performance improvements is  
182 a better partitioning of turbulent fluxes [Davin *et al.*, 2011; Davin and Seneviratne, 2012].

183 Both simulations were integrated using a horizontal resolution of 0.22° (~25km), a vertical  
184 resolution of 32 pressure levels and a 120s time step. The model grid covers all of Western  
185 Europe (Figure 1) and consists of 170 x 180 pixels in respectively latitude and longitude. Both  
186 simulations were integrated from 1 July 2002 to 1 January 2009, a time period which covers  
187 the available observations and includes a 6 month spinup period before the first available  
188 measurement year (2003). Initial and boundary conditions were derived from ERA-Interim  
189 Reanalysis data.

### 190 **2.3 Model Experiment**

191 In this study, the model experiment required two simulations. In the first simulation (the  
192 “forest” simulation), the seven pixels matching the seven locations of the observational pairs  
193 were prescribed as forest. In the second simulation (the “open land” simulation), the same  
194 seven pixels were set to grassland or crop depending on the surface above which the  
195 FLUXNET mast was installed.

196 When doing a standard simulation with CLM3.5, values that describe the land surface are  
197 derived from input datasets [Lawrence and Chase, 2007]. Surface input variables required for  
198 CLM3.5 include plant functional type (PFT), canopy top and bottom height, leaf area index  
199 (LAI), stem area index (SAI), soil color and soil texture. For this study, three of these input  
200 variables were adapted to local measurement site conditions: PFT, canopy top height and LAI.  
201 Values for these adaptations are summarized in Table 2. First, for PFT, one in four options  
202 was chosen depending on land use (forest or open land) and dominant tree species: needleleaf  
203 evergreen tree – temperate or broadleaf deciduous tree – temperate on the forest side and C3  
204 grass or crop on the open land side. Second, the input variable canopy top height was adapted  
205 to the observational sites for the forest simulation only. For the open land simulation, the  
206 standard CLM3.5 value for grassland and cropland of 0.5 m was used. Finally, CLM3.5 uses a  
207 yearly cycle of LAI which is updated daily by interpolating between monthly values [Oleson  
208 *et al.*, 2004]. For the forest sites, these monthly LAI values were adjusted to match the local  
209 site conditions more closely.

### 210 **2.4 Data processing**

211 The observational datasets were downloaded from the European Fluxes Database Cluster  
212 (<http://www.europe-fluxdata.eu/>). For this study, level 2 data products were used throughout.  
213 These data products provide values on a half-hourly timescale, and are quality checked by the  
214 site PI, but have not been through any gapfilling. Further data processing was required for the  
215 aims of this study. For all variables three subsets were created. One subset containing daily  
216 mean values, another containing the daytime mean and the last subset containing nighttime  
217 mean values. This approach enabled separately studying nighttime and daytime climate as  
218 well as evaluating the effect when this distinction is not made and daily means are used  
219 instead.

220 For the daily mean subset, a mean daily value was calculated for every variable from the half-  
221 hourly level 2 product. Days with measurement gaps longer than 3 hours were removed from  
222 the dataset. For the daytime mean subset, a mean daily value was calculated for all  
223 observation from 12:00 to 15:00 UTC. If one of the 6 half-hourly measurements within this  
224 window was missing, the whole day was omitted from the daytime mean subset. A similar  
225 procedure was used to calculate the nighttime subset, except here, the 00:00 to 03:00 UTC  
226 time window was used. All of the following data processing steps were performed on these  
227 three subsets:

228 (1) Albedo and surface emissivity were calculated for sites with separate measurements for  
229 incoming and outgoing shortwave and longwave radiation. Surface albedo ( $\alpha_s$ ) was  
230 determined by computing the ratio between outgoing and incoming shortwave radiation for  
231 the daytime mean subset (12:00-15:00 UTC). Next, surface emissivity  $\epsilon_s$  was derived from  
232 surface albedo using a simple linear equation ( $\epsilon_s = 0.16 \alpha_s + 0.99$ ). This empirical  
233 relationship was derived from literature reported values of albedo and emissivity [*Juang et al.*,  
234 2007].

235 (2) For sites with separate measurements for incoming and outgoing longwave radiation,  
236 radiative surface temperature ( $T_s$ ) was derived from outgoing longwave ( $LW_{out}$ ) using Stefan  
237 Boltzman's equation ( $LW_{out} = \epsilon_s \sigma T_s^4$ ).

238 (3) Observed energy budgets are rarely closed and imbalances of up to 20% of available  
239 energy are common [*Wilson et al.*, 2002]. It has been suggested that one of the most  
240 prominent sources for this imbalance is an underestimation of the turbulent fluxes, caused by  
241 the fact that the eddy-covariance method tends to miss or underestimate large scale eddies  
242 [*Foken*, 2008]. Therefore, the surface energy budget was closed by redistributing the

243 imbalance term (incoming terms minus outgoing terms) to sensible and latent heat, with the  
 244 fraction of the imbalance allocated to each term determined by the measured Bowen ratio  
 245 (relative proportion of sensible to latent heat). Note that this means we assume the Bowen  
 246 ratios for small and large scale eddies are similar. Although this might not hold in all cases  
 247 [Ruppert *et al.*, 2006], the redistribution of the imbalance based on Bowen ratio is the only  
 248 method easily applicable to our observational dataset.

249 (4) As we aim to compare the climatology of nearby sites, the difference between the values  
 250 observed at the forest site and the nearby open land site were calculated. We chose to subtract  
 251 the forest site value from the open land value, so the calculated difference value therefore  
 252 reflects the change associated with deforestation. The output data from our model simulations  
 253 was processed in a similar fashion with the sole exception that by conception the energy  
 254 budget of COSMO-CLM<sup>2</sup> is closed and no imbalance correction (see step (3)) was required.

## 255 **2.5 Decomposition of surface temperature change**

256 To decompose the observed change in radiative surface temperature (Ts) between forested  
 257 and open land sites, the method originally developed by Juang *et al.* [2007] was used. This  
 258 method has been refined [Luyssaert *et al.*, 2014] and subsequently been applied by others  
 259 [Luyssaert *et al.*, 2014; Akkermans *et al.*, 2014; Thiery *et al.*, 2015]. The decomposition uses  
 260 the basic surface energy budget equation as its starting point:

$$\epsilon_s \sigma T_s^4 = [1 - \alpha_s] SW_{in} + LW_{in} - LE - H - G - I \quad (1)$$

261 By reordering the equation and performing a first order derivative, the decomposition  
 262 equation for  $\delta T_s$  or the difference in surface temperature between two sites is obtained:

$$\delta T_s = \frac{1}{4\epsilon\sigma T_s^3} [-SW_{in}\delta\alpha_s + (1 - \alpha_s)\delta SW_{in} + \delta LW_{in} - \delta LE - \delta H - \delta G - \delta I - \sigma T_s^4 \delta \epsilon_s] \quad (2)$$

263 1 2 3 4 5 6 7 8

264 This equation is then applied to our site pairs, which reflect a local land use transition from  
 265 forest to open land. Using the equation, we can attribute the change in surface temperature to  
 266 eight factors:

267 1. Albedo ( $\alpha_s$ ). A positive value implies that the open land site is darker than the forest, and  
 268 therefore, absorbs a larger fraction of the incident solar radiation.

269 2. Incoming shortwave radiation (SW<sub>in</sub>). A positive value implies that the incoming  
 270 shortwave radiation is higher over the open land site. Possible mechanisms could be

271 feedbacks including changes in atmospheric moisture, atmospheric aerosol loading, cloud  
272 cover, etc.

273 3. Incoming longwave radiation (LWin). A positive value implies that the incoming longwave  
274 radiation is higher over the open land site. Possible mechanisms could be changes in cloud  
275 cover, atmospheric aerosol loading, water vapor loading in the lower boundary layer, etc.

276 4. Latent heat flux (LE). A positive value implies that the latent heat flux, and therefore, the  
277 evaporative cooling of the surface, is lower for the open land site.

278 5. Sensible heat flux (H). A positive value implies a reduction in convective surface cooling.

279 6. Ground flux (G). A positive value implies reduced soil heat storage.

280 7. The imbalance term (I). The imbalance term accounts for the imbalance as discussed above  
281 as well for the omission of minor components of the energy budget such as heat storage in  
282 biomass, heat storage in sub-canopy air mass and energy used in photosynthesis. Ideally, this  
283 component should approach zero, but for observational data, this is almost never the case.

284 8. The thermal emissivity of the surface ( $\epsilon_s$ ). A positive value implies an increase in the  
285 surface emission of longwave radiation due to an increase in emissivity, with the surface more  
286 closely resembling a black-body radiation.

287 For the observational data subsets, the surface temperature decomposition equation was  
288 applied twice: once using the original uncorrected values for sensible and latent heat, and then  
289 again using the values corrected for imbalance. The differences between these values can be  
290 interpreted as a measure of the uncertainty related to measuring turbulent fluxes.

291 Applying the equation to both observations and modeled site pairs results in a daily value for  
292  $\delta T_s$ , calculated from the observed and modeled differences in all surface energy budget  
293 components. For COSMO-CLM<sup>2</sup>, this calculated value matches the actual daily mean  $\delta T_s$   
294 value closely across the board. However, this is not the case when the surface temperature  
295 decomposition equation is applied to our observational site pairs. Here, large discrepancies  
296 exist between calculated and observed  $\delta T_s$  reflecting uncertainties in the measurements.  
297 Consequently, we can use the difference between the calculated and the observed value of  $\delta T_s$   
298 as an estimate for data reliability.

299 As mentioned earlier, a surface energy budget closure imbalance of about 20% of available  
300 energy is common in measurements [Wilson *et al.*, 2002]. For our site pairs, this corresponds  
301 to an imbalance of about  $11 \text{ W m}^{-2}$ , or 2 K when translated to temperature using equation 2.

302 Therefore, 2 K was chosen as a cutoff value for calculated minus observed  $\delta T_s$  ( $\delta T_{\text{scal}} -$   
303  $\delta T_{\text{sobs}}$ ). Days where ( $\delta T_{\text{scal}} - \delta T_{\text{sobs}}$ ) is lower than this cutoff value are deemed reliable,  
304 days that do not meet this criterion are not. This data reliability measure was applied  
305 separately to all three data subsets created for our observational site pairs. For a site pair, at  
306 least 25% of the days for which the decomposition method was applied had to pass the 2 K  
307 threshold to be included in the final data set.

## 308 **2.6 Data availability and quality**

309 Despite the length of the time series, our additional criteria to data quality and availability  
310 (see section 2.5) considerably reduced the size of the data (Table 3). For example, for the CZ1  
311 site pair, 3 years of common measurements are available. However, only 38 percent of days  
312 within this common measurement period have  $T_a$  measurements for both sites within the site  
313 pair.

314 LWout is an important variable because it is essential in calculating surface temperature ( $T_s$ ).  
315 Since we use the difference between the calculated and the observed value of  $T_s$  as a measure  
316 for data reliability, this means that site pairs with no common measurements of LWout cannot  
317 pass our reliability test. For most site pairs, however, LWout is the variable with the least  
318 consistent coverage, and thus the most limiting. Two pairs (PT1 and ES1) out of seven have  
319 no common LWout measurements at any time. For two other pairs (IT1 and CZ1) common  
320 measurements of LWout are mostly restricted to summer. Coverages of ~40%, ~80%, and,  
321 ~95% respectively, make DK1, DE1 and IT2 the only three pairs remaining for the core of the  
322 analysis. Site pairs DE1 and DK1 have the highest fraction, i.e. 55 to 75% of reliable  
323 measurements (Figure 2), where reliability is calculated as the number of days for which  
324 ( $\delta T_{\text{scal}} - \delta T_{\text{sobs}}$ ) is less than +/- 2 K. For the IT2 site pair, data reliability is lower overall,  
325 and less consistent across time of day.

326 A possible reason for the lower fraction of reliable site comparisons at site pairs IT2 is the  
327 substantial elevation difference of the sites within this pairs. For IT2, the open land site is  
328 located 210 meters higher than the forest site. Whereas, height differences for DE1 and DK1  
329 are only 100 and 30m, respectively.

330 It is, however, worth noting that despite the low percentages of high quality data, sample size  
331 is adequate for our purpose thanks to the relatively high number of years with common  
332 measurements for these site pairs. The daily mean reliable year-round subset, for example,  
333 still contains 1570 days when summed across site pairs 1-3. The lowest absolute number of

334 days can be found in the summer daytime mean subset, which still contains 243 entries (Table  
335 3).

### 336 **3 Results**

#### 337 **3.1 Difference in temperature**

338 The yearly mean daytime difference in air temperature ( $\delta T_a$ , with  $T_a$  typically measured  
339 approximately 2 m above the vegetation canopy) does not differ significantly from zero ( $p =$   
340 0.71), being equal to about 0.02 K (Figure 3). Note that these values are uncorrected for the  
341 height difference between the sites within pairs. Based on a possible lapse rate range of 5.5 -  
342 10 K/km, we calculated a weighted average  $\delta T$  due to height difference of -0.53 to -0.96 K. In  
343 the subsequent analysis,  $\delta T$  values in the 0 to -0.96 K range should therefore be considered to  
344 be insignificant from zero. The daytime  $\delta T_a$  due to deforestation is simulated reasonably well  
345 by COSMO-CLM<sup>2</sup>: agreement is strong, with the model replicating the observed seasonal  
346 cycle almost perfectly (Pearson correlation, 0.94). The difference in daytime  $T_s$  is  
347 characterized by a strong seasonal signal: in winter,  $\delta T_s$  for open land sites is cooler by about  
348 1.5 K, while in spring and summer, open land sites are warmer by up to 3 K. Summer  
349 warming is stronger and longer in duration, dominating the yearly mean daytime  $\delta T_s$  signal.  
350 The model produces a seasonal pattern similar to observations: open land sites are cooler than  
351 forests in winter and warmer in summer. COSMO-CLM<sup>2</sup> does somewhat underestimate the  
352 magnitude of summer open land warming.

353 Moving on to nighttime, yearly mean nighttime  $\delta T_a$  equals about -1.3 K, suggesting that the  
354 atmosphere above open land is cooler than above forest with minimal seasonal variation.  
355 COSMO-CLM<sup>2</sup> does not succeed at simulating this observed nighttime  $\delta T_a$ , overestimating  
356 yearly mean nighttime  $\delta T_a$  by about 1.5 K. The difference in nighttime  $\delta T_s$  does show  
357 seasonal variation: in winter open land site  $T_s$  is lower by up to 5.5 K while in late summer  
358 and fall, open land sites are still cooler but the difference is reduced to 2.5 K. It is worth  
359 noting, however, that the seasonal amplitude in nighttime  $\delta T_s$  is significantly smaller for the  
360 dataset containing all data. Still, the fact that open land sites are cooler during nighttime than  
361 nearby forests is robust across pairs. Similar to nighttime  $\delta T_a$ , COSMO-CLM<sup>2</sup> does a poor  
362 job in simulating the observed nighttime  $\delta T_s$  with a bias of 4K between the simulated and  
363 observed values. These nighttime biases are large enough to reverse the sign of nighttime  $\delta T_s$   
364 compared to the observations: unlike in the observations, in our COSMO-CLM<sup>2</sup> simulations,  
365 open land sites are warmer than forests at night, especially in spring.

366 Finally, daily mean  $\delta T_a$  hovers at around -0.8 K, with little to no seasonal variation. It is  
367 driven primarily by the difference in nighttime temperature, which is considerably higher in  
368 magnitude than the observed daytime temperature difference. COSMO-CLM<sup>2</sup> overestimates  
369 daily mean  $\delta T_a$  by about 0.5 K due to the  $\delta T_a$  overestimation at night. Daily mean  $\delta T_s$  is also  
370 negative year round. Its seasonal signal (about -3.5 K in winter, close to zero in summer) is  
371 determined mostly by daytime  $\delta T_s$ , while its sign (negative year round) is determined mostly  
372 by nighttime  $\delta T_s$ . In COSMO-CLM<sup>2</sup>, daily mean  $\delta T_s$  is overestimated by about 2K, again  
373 mainly because of the nighttime bias.

## 374 **3.2 Surface temperature change decomposition**

### 375 **3.2.1 Daytime/ summer**

376 Using the  $\delta T_s$  decomposition equation, changes in  $T_s$  were attributed to changes in the  
377 components of the surface energy budget (Figure 4). For summer days, the difference in  
378 albedo between open land and forested sites appears to be a dominant factor in changes in  
379 surface temperature. Albedo is higher for open land sites, where the difference in albedo was  
380 estimated to be equivalent to a  $\delta T_s$  of -6 K. This difference is modeled accurately by  
381 COSMO-CLM<sup>2</sup> in both sign and magnitude (Figure 4a). For the observed pairs, summer days  
382 are thus characterized by a lower net radiation ( $R_{net}$ ) at the open site compared to the forest.  
383 However, the surface responds to deforestation by simultaneously reducing the sensible heat  
384 flux ( $H$ ), a reduction which, if isolated, would cause a surface heating of 6 to 8 K. This  
385 reduction in  $H$  is consistent with a decrease in surface aerodynamic roughness ( $R_s$ ), common  
386 for deforestation. The reduction in  $H$  more than offsets the cooling through increased albedo,  
387 causing the observed surface warming of 2 K. Consistent with a decrease in surface  
388 aerodynamic roughness and possibly, due to a shallower rooting system,  $LE$  was also  
389 observed to decrease with an effect on  $T_s$  ranging between 0 and 5 K (corrected for lack of  
390 SEB closure and uncorrected, respectively).

391 The interplay between albedo driven cooling and roughness-driven warming following  
392 deforestation is reasonably well represented in COSMO-CLM<sup>2</sup>. Contrary to observed  
393 however, modeled warming due to a reduction in  $H$  does not exceed albedo cooling. In  
394 COSMO-CLM<sup>2</sup>, both counteracting processes are of equal magnitude (+6 K versus -6 K). The  
395 model and observations differ most in the difference in incoming shortwave radiation from  
396 the atmosphere ( $SW_{in}$ ) to the vegetation. The difference due to  $SW_{in}$  is small and statistically  
397 insignificant ( $p = 0.50$ ) for the observational site pairs, but very important in our model  
398 simulations. In COSMO-CLM<sup>2</sup>, increased  $SW_{in}$  (+7 K) is offset only partially by increases in

399 both LE and ground flux (G) (-2.5 K to -3 K each). The result is a surface warming of about 1  
400 K. For summer days, COSMO-CLM<sup>2</sup> thus simulates a correct change in surface temperature  
401 due to deforestation, but the underlying processes are somewhat different.

402 As shown in Figure 5a, the increase in modeled incoming shortwave radiation present in our  
403 COSMO-CLM<sup>2</sup> simulations is a feature that is present in all 7 site pairs, not just the 3 site  
404 pairs with reliable measurements included in the temperature change decomposition analysis.  
405 Figure 5a also shows that the increase is highest in summer and lowest in winter. The increase  
406 in SWin appears to be caused by a decrease in cloud cover ( $\delta$ CLC), and specifically, in  
407 medium (not shown) and low level clouds (dCLC, Figure 5b). This is evidenced by the fact  
408 that the peak in  $\delta$ SWin seem to coincide well with the negative peak in  $\delta$ CLC.

### 409 **3.2.2 Daytime/ winter**

410 The effect of deforestation on winter surface temperature is simulated correctly in COSMO-  
411 CLM<sup>2</sup>; with the model simulating a surface cooling of 2 K, consistent with observations  
412 (Figure 4b). Similar to summer daytime, the difference in albedo drives the observed and  
413 simulated changes. However COSMO-CLM<sup>2</sup> underestimates the magnitude of the associated  
414 cooling of the open land compared to forest. The model simulates a  $\delta$ Ts due to albedo of  
415 about -4 K, as opposed to -8 K for the observations. This presents a departure from the  
416 model's behavior in summer, where the modeled effect of changes in albedo reasonably  
417 matched the observations. The difference in observed and modeled albedo is likely related to  
418 a mismatch between observed and simulated snow cover, rather than a deficiency in how  
419 plant canopy albedo is parameterized. This is supported by the fact that for the open land sites  
420 in our observational dataset, 21% of winter days with reliable measurements have a surface  
421 albedo higher than 0.5, typical for a snow surface. In our model simulations, this is only the  
422 case for 5% of winter days.

423 The observational data show that deforestation is associated with a decrease in H, triggered by  
424 both the reduction in Rnet and lower surface aerodynamic roughness and resulting in a  
425 surface warming of 5 to 8 K. COSMO-CLM<sup>2</sup> also simulates a decrease in H, albeit smaller in  
426 absolute value (2.5 K). However, relative to albedo cooling, the decrease in H is similar in  
427 both model and observations (66 to 100% of albedo cooling for the observations versus 60%  
428 of albedo cooling for COSMO-CLM<sup>2</sup>). Finally, deforestation is characterized by a small  
429 decrease in LE in both observations and COSMO-CLM<sup>2</sup>, triggered by a combination of lower  
430 Rnet, lower surface aerodynamic roughness and a shallower rooting system. The model does  
431 not match the observed changes in SWin and G though: whereas observed SWin shows a

432 small decrease and no change in G, model simulations show a small increase in SWin and a  
433 small increase in G.

434 Overall, we can conclude that COSMO-CLM<sup>2</sup> simulates the observed  $\delta T$ s during winter days  
435 accurately, and moreover, is correct in its simulation of the underlying mechanisms: albedo-  
436 induced cooling partially offset by a decrease in sensible heat flux is the dominant mechanism  
437 during winter days for both model and observations. COSMO-CLM<sup>2</sup> does underestimate the  
438 magnitude of albedo-induced cooling due to an underestimation in the amount of snow events  
439 compared to observations.

### 440 **3.2.3 Nighttime**

441 During nighttime, open land sites are observed to be significantly cooler than nearby forested  
442 sites (Figure 6) during both summer (-2 K) and winter (-5 K). This LUC effect is completely  
443 missing from our COSMO-CLM<sup>2</sup> simulations. In COSMO-CLM<sup>2</sup>, open land nighttime  
444 temperatures are statistically equal to nearby forest temperatures during summer ( $p = 0.13$ ),  
445 and only slightly lower during winter. The biggest difference between model and observations  
446 is in the incoming longwave radiation component (LWin). For our observational site pairs  
447 LWin over the open land site is considerably lower than over the nearby forested site. The  
448 cooling associated with this reduction in LWin ranges from 1.5 to 2.1 K, for summer and  
449 winter respectively. In our model simulations, the cooling associated with this factor is  
450 smaller, ranging from 0.1 to 0.5 K.

451 Monthly boxplots for the difference in nighttime incoming longwave radiation ( $\delta LWin$ ) are  
452 shown in Figure 7 for both model and observations. On the observational side, mean  $\delta LWin$   
453 across all reliable data equals  $-7.8 \text{ Wm}^{-2}$  and is statistically different from zero ( $p < 1E-15$ ).  
454 The 75th percentile of  $\delta LWin$  is below zero for all but three months, pointing towards a broad  
455 yearlong trend of decreased LWin following deforestation. On the other hand, COSMO-  
456 CLM<sup>2</sup> simulations are characterized by a mean  $\delta LWin$  of only  $-0.9 \text{ Wm}^{-2}$ , a difference which  
457 is not statistically different from zero ( $p = 0.10$ ). Therefore, we can conclude that in our  
458 simulations, no broad yearlong trend towards a decrease in LWin exists.

459 Model and observations disagree over the change in G as well, and the disagreement observed  
460 in this component contributes to explaining why simulated and observed  $\delta T$ s differ. In  
461 summer, both observations and simulations have a lower (more negative) G for open land  
462 sites compared to forests. In other words, heat loss of soils to the surface is more important for  
463 open land than for forest. However, COSMO-CLM<sup>2</sup> overestimates this effect by almost 1 K.

464 In winter, the observed difference in ground flux between open land and forested sites is  
465 significant on the 0.05 level but very small ( $p = 0.10$ ) whereas in COSMO-CLM<sup>2</sup> open land  
466 sites still have more ground heat release, causing a surface warming of about 2 K.

467 The observed and modeled mean daily cycle of G during winter for forest and open land are  
468 shown in Figure 8. The observed G is characterized by minimal diurnal variation, remaining  
469 slightly negative throughout. This is true for both open land and forest sites, as both lines are  
470 virtually identical. Modeled G, however, is characterized by considerable diurnal variation,  
471 from highly positive during daytime to negative at night. Moreover, modeled G differs  
472 between forests and open land, resulting in a nighttime difference in surface warming not  
473 present in reality. It is worth noting that, at least in part, this disagreement between model and  
474 observations could be related to the modeled underestimation in wintertime snow cover (as  
475 mentioned in section 3.2.2), since snow tends to insulate the soil column.

476

477 Observations and simulations do agree on the contribution caused by the sensible heat  
478 component (H). At night, as the surface cools, a stable reverse stratification usually forms in  
479 the nocturnal boundary layer. Turbulence can disrupt this stable stratification, and bring heat  
480 from aloft to the surface. However, open land sites are characterized by a decreased surface  
481 roughness and thus, a decrease in turbulence. This is observed at our observational pairs: the  
482 open land sites are characterized by a higher H, which at night means less negative, leading to  
483 a mean cooling of 2.2 to 3 K compared to forests, depending on season. COSMO-CLM<sup>2</sup> is  
484 able to simulate this behavior with the associated cooling matching observations in winter and  
485 slightly underestimating this process by 0.8K in summer.

## 486 **4 Discussion**

### 487 **4.1 Daily cycle of the observed temperature difference between forest and** 488 **grassland.**

489 Owing to the strict requirements for data quality and availability, our study could only make  
490 use of three to seven observational pairs depending on the analysis. Representativeness of our  
491 analysis of few sites was tested against the body of literature on the topic. A strong latitudinal  
492 dependency of the drivers of  $\delta T$  is emerging from literature study. For the tropical zone, most  
493 studies agree that deforestation causes a warming of local climate because here, the warming  
494 effect of a decrease in evapotranspiration tends to outweigh the cooling effect of a higher  
495 albedo (e.g.[*Randow et al.*, 2004]). This first order effect of deforestation has been

496 successfully reproduced by several modeling studies [*Davin and de Noblet-Ducoudré*, 2010;  
497 *Nogherotto et al.*, 2013; *Akkermans et al.*, 2013; *Akkermans et al.*, 2014; *Lejeune et al.*, 2014].  
498 Conversely, in the boreal zone, most observational studies agree that deforestation leads to a  
499 cooling of local climate, because here, the increase in albedo due to the highly contrasting  
500 albedo during the snow season dominates the temperature response (e.g. [*Randerson et al.*,  
501 2006]). Temperate climate zones, such as in Europe where this study was located, are  
502 characterized by a  $\delta T$  response that is in between these two extremes. Just like in the tropical  
503 and boreal climate zones, open land surfaces tend to be brighter than forests, a cooling effect  
504 that increases with latitude due to the increasing presence of winter snow cover. Two other  
505 mechanisms have the potential to cause an opposing surface warming: a reduction in turbulent  
506 surface cooling due to reduced surface roughness and decreased evapotranspiration due to  
507 both reduced roughness and a shallower rooting system.

508 Despite observational evidence remaining limited, most studies using observational data for  
509 temperate regions (e.g. Europe, most of North America, parts of Asia) agree on the  
510 aforementioned biogeophysical mechanisms (Table 4). Disagreement does exist over the sign  
511 of the yearly mean  $\delta T$  signal. Some observational studies conclude that winter cooling is  
512 strong enough to dominate the yearly mean  $\delta T$  signal, or in other words, that on a yearly mean  
513 scale deforestation leads to surface cooling [*Lee et al.*, 2011; *Zhang et al.*, 2014]. *Baldocchi et*  
514 *al.* [2013] also report cooling, but the dominant mechanisms here are somewhat different.  
515 Other observational studies conclude that the summer decrease in LE and/or H and associated  
516 summer warming following deforestation is strong enough to cause a positive yearly mean  
517 signal for  $\delta T$  (e.g. [*Juang et al.*, 2007; *Montes-Helu et al.*, 2009]).

518 The studies cited here are some of the only observational studies performed for temperate  
519 zones that simultaneously study the effect of deforestation on both surface temperature and  
520 the full surface energy budget. The fact that some studies associate deforestation with surface  
521 warming while others observe cooling supports the hypothesis that in temperate regions, the  
522 yearly mean  $\delta T$  signal is the results of opposing mechanisms and can go towards either  
523 warming or cooling depending on local conditions [*Pitman et al.*, 2011; *Luyssaert et al.*,  
524 2014]. Interestingly, results from modeling studies using global climate model simulations  
525 tend to be more one sided. These studies generally agree that deforestation in temperate regions  
526 leads to surface cooling [*Snyder et al.*, 2004; *Brovkin et al.*, 2006; *Bala et al.*, 2007; *Davin*  
527 *and de Noblet-Ducoudré*, 2010]. One possible reason could be the large scale of deforestation  
528 utilized in these simulations, when compared to the scale of deforestation typical for

529 observational studies. These large scale deforestations could trigger atmospheric and/or ocean  
530 feedbacks in global climate models that do not occur after deforestations smaller in scale (e.g.  
531 a sea-ice feedback). Second, we speculate that these model simulations do not fully capture  
532 the varied observed impact of deforestation because they lack the variety in land use subtypes  
533 present in reality.

534 The seven observational pairs used in this study are characterized by a yearly mean  $\delta T$  of  
535 about -2.5 K, and are thus in line with the global climate modeling studies and other  
536 observational studies reporting cooling. However, it is worth noting that so far, we have only  
537 discussed the daily mean climate effect of deforestation. Few studies distinguish between  
538 daytime and nighttime climate when analyzing the effect of deforestation on temperature, like  
539 we did here. Only two such studies could be found using observational data for climate zones  
540 similar to our European study area: a study for North America conducted by *Lee et al.* [2011]  
541 and a follow up study performed by *Zhang et al.* [2014] for Eastern Asia. In concordance with  
542 our results, these studies confirm the importance of differentiating between daytime and  
543 nighttime climate when analyzing  $\delta T$  caused by deforestation.

544 *Lee et al.* [2011] compared 2m air temperature for 37 open land/ forest site pairs across North  
545 America. A surface energy budget analysis showed that daytime  $\delta T_a$  following deforestation  
546 is determined by the balance between two processes also described in this study: warming due  
547 to suppression of turbulent fluxes versus cooling due to increased albedo. For site pairs in the  
548 28°-45° N latitudinal range the effect of these two processes on  $T_a$  offset each other perfectly.  
549 In the 45°-56° N latitudinal range, albedo induced cooling is stronger and is able to overcome  
550 warming due to turbulent suppression. The daytime specific  $\delta T_a$  values and the responsible  
551 processes reported in this study for European site pairs seem to coincide well with these  
552 observed North American values. The mechanisms responsible for the temperature  
553 differences are the same mechanisms we discussed when giving an overview of the daily  
554 mean effect of deforestation.

555 The storyline does change when moving the analysis to nighttime. Few studies report  
556 nighttime  $\delta T_a$  values, but the ones that do all report that deforestation leads to a nighttime  
557 cooling in the order of -1 to -2 K (Table 4). Values for  $\delta T_a$  reported here are similar, at -2 K  
558 uncorrected and -1 K with extreme lapse rate correction for the data subset using all site pairs.  
559 Both *Lee et al.* [2011] and *Zhang et al.* [2014] also touch briefly on the mechanism  
560 responsible for these differences, speculating that open land is cooler at night because forests  
561 can bring more heat from aloft to the surface due to increased turbulent mixing. However,

562 neither study provides any evidence backing up this hypothesis. As shown here in section 3.2,  
563 the nighttime cooling associated with deforestation observed in our site pairs seems to be the  
564 result of a combination of factors. The first mechanism responsible for nighttime cooling is a  
565 decrease in incoming longwave radiation. Second, a decrease in turbulent mixing (evidenced  
566 by a higher, less negative mean H at night) is observed, confirming the mechanism suggested  
567 by *Lee et al.* [2011]. At night, forests thus warm the surface through increased roughness,  
568 turbulence and vertical advection. A similar mechanism was reported by *Wouters et al.* [2013]  
569 for built-up urban environments.

570 Important to note however, is that these studies show that nighttime  $\delta T_a$  values are essential  
571 in explaining observed yearly mean  $\delta T_a$ . For example, our results show that without nighttime  
572 cooling, yearly mean daily  $\delta T$  following deforestation would be positive instead of slightly  
573 below zero. The same is true for the North-American site pairs studied by *Lee et al.* [2011] in  
574 the 28°-45° N latitudinal range. To conclude, there are clearly important mechanisms at play  
575 at night which are unrelated to the mechanisms commonly associated with deforestation in  
576 studies which focus only on daily mean effects. These mechanisms are important in  
577 explaining daily mean  $\delta T_a$ , and should therefore be accounted for.

#### 578 **4.2 Added value of methodology based on temperature decomposition**

579 As mentioned in the introduction, the methodology as applied in this study, which combines  
580 simulations with a coupled land-atmosphere, a direct sensitivity analysis evaluating the  
581 changes associated with deforestation, a separate analysis for daytime and nighttime and  
582 temperature decomposition is a novel way of evaluating the impact of LUC in climate models.  
583 It moves past simple bias description by investigating the biogeophysical mechanisms  
584 responsible for surface temperature differences in both model and observations. This is  
585 accomplished by calculating the sensitivity of changes in surface temperature to changes in  
586 the component of the energy budget, i.e., albedo, latent heat, sensible heat, incoming  
587 shortwave radiation, ground heat and ecosystem emissivity.

588 The underlying idea of this method is that LUC triggers changes in the biogeophysical  
589 interactions between the land surface and the atmosphere. For example, forests have deeper  
590 and more complex rooting systems compared to grasses or crops, and therefore, are likely to  
591 maintain higher evapotranspiration rates under dry conditions. This example illustrates that  
592 changes in biogeophysical properties following LUC have a direct or indirect impact on one  
593 or multiple components of the surface energy budget. In this particular example, the SEB  
594 component most affected will be latent heat flux. In turn, any change in a SEB component

595 triggers, if isolated, a change in near surface temperature. For example, higher  
596 evapotranspiration rates, if not compensated by changes in other surface energy budget terms,  
597 will lead to lower near surface temperatures due to evaporative cooling. Note though that the  
598 method decomposes the net effects of LUC. Gross effects and feedbacks resulting in the net  
599 effect remain hidden.

600 The decomposition method described here allows us to determine whether our model gives  
601 acceptable results for  $\delta T_s$  following LUC, or in other words whether the model is simulating  
602 correct  $\delta T_s$  values for the right biogeophysical reasons. The decomposition method also helps  
603 establishing whether incorrect  $\delta T_s$  values are due to large biases in several biogeophysical  
604 mechanisms, due to the result of a modest underestimation in just one of the important  
605 mechanisms, or alternatively, simply due to one or more observed biogeophysical  
606 mechanisms that are not modeled. These results are summarized in Table 5.

607 For winter days, COSMO-CLM<sup>2</sup> is able to simulate correct  $\delta T_s$  values for the right reasons,  
608 with both model and observations showing a similar cooling following deforestation due to  
609 higher albedo partially offset by a reduction in turbulent fluxes. For summer days, both model  
610 and observations showed warming following deforestation, but the model simulations include  
611 a mechanism raising  $S_{Win}$  that was not confirmed by the observations.

612 Nighttime  $\delta T_s$  values were clearly biased, largely underestimating the observed nighttime  
613 cooling following deforestation. Biases in two distinct mechanisms are responsible for this  
614 underestimation: an underestimation of the reduction in  $L_{Win}$  and an overestimation of the  
615 increase in heat storage release. It is worth noting though that a third important nighttime  
616 mechanism, a decrease in turbulent mixing, was found to be well represented.

### 617 **4.3 Difference in nighttime $L_{Win}$**

618 Why do we observe a lower  $L_{Win}$  over open land at night (Figure 7)? One possible  
619 explanation is a decrease in water vapor in the nocturnal boundary layer (NBL), compared to  
620 forests. It is well known that water vapor acts as a greenhouse gas, limiting the escape of  
621 longwave radiation through the atmosphere [Christy *et al.*, 2006]. It can also cause swelling of  
622 hygroscopic aerosols, further increasing  $L_{Win}$  in situations where there are substantial  
623 emissions of aerosols into the NBL [Nair *et al.*, 2011]. However, only limited evidence of  
624 lower water vapor content over open land exists in our measurements. Nighttime specific  
625 humidity measured over forest and open land (usually only a few meters above vegetation for  
626 flux measurement sites) is comparable for the DE1 site pair and is somewhat lower over open

627 land for the IT2 site pair (-0.4 g/kg or -12% in winter and -1.4 g/kg or -14% in summer). No  
628 paired humidity measurements exist for the DK1 site pair. The observations thus do not  
629 provide conclusive evidence for a decrease in LWin over open land due to decreased water  
630 vapor loading. Answering this question more conclusively would require more measurements  
631 higher up in the boundary layer.

632 One other factor which could explain reduced nighttime LWin over open land is a difference  
633 in NBL aerosol loading. Most studies into the effect of atmospheric aerosols focus on daytime  
634 (e.g. [Bellouin *et al.*, 2005; Takemura *et al.*, 2002]). During daytime, aerosols tend to have a  
635 cooling effect on surface temperature due to: 1) the direct effect of increased scattering and  
636 absorption of shortwave solar radiation and 2) the indirect effect on cloud formation (aerosols  
637 act as cloud condensation nuclei) [Yu *et al.*, 2002]. There are few studies focusing on the  
638 effect of aerosols on nighttime surface climate. One recent study by Nair *et al.* [2011] did  
639 focus on nighttime, using a one-dimensional version of a regional climate model to assess the  
640 effect of urban aerosols on radiative forcing and surface air temperature. The results showed  
641 that urban aerosols have a statistically significant impact on nighttime downwelling longwave  
642 radiation at the surface, increasing LWin by 2.7 to 47 Wm<sup>-2</sup>, depending on the scenario used.

643 We therefore hypothesize that the difference in nighttime LWin observed for site pairs DE1  
644 and IT2 could be related at least in part to a difference in NBL aerosol loading. Forests emit  
645 large quantities of biogenic volatile organic compounds (BVOC's) into the atmosphere, which  
646 then in turn contribute to the formation of large secondary organic aerosols (SOA) [Ehn *et al.*,  
647 2014; Carslaw *et al.*, 2010]. Studies for boreal forests (where anthropogenic air pollution is  
648 minimal) have shown that these biogenic SOA can have a large local impact on the radiative  
649 budget [Kurten *et al.*, 2003; Spracklen *et al.*, 2008]. Recently, a modeling study has estimated  
650 the impact of global historic cropland expansion through BVOC emissions at a cooling  
651 equivalent to  $-0.11 \pm 0.17$  Wm<sup>-2</sup> [Unger, 2014]. However, these studies focus mainly on the  
652 impact of aerosols on shortwave scattering and cloud formation. So far, a detailed analysis  
653 into the impact of biogenic aerosols on nighttime radiative forcing over forests has not yet  
654 been performed.

655 Finally, higher values of nighttime LWin over forests could be related to the enhanced  
656 entrainment of warm air reported in the results section. As mentioned above, forests, owing to  
657 their higher aerodynamic roughness, generate more turbulence, evidenced by a lower (more  
658 negative) mean nighttime sensible heat flux (Figure 6). As shown by Walters *et al.* [2007],  
659 any perturbation in a weakly stable nocturnal boundary layer can trigger a shift from a stable

660 temperature profile to a turbulent regime, mixing warm air from aloft and significantly  
661 increasing (near) surface temperature. Assuming the advection of warmer air closer to the  
662 surface increases surface LWin, the higher nighttime LWin observed over forests could  
663 simply be related to the increased occurrence of this type of disruptive events. If true,  
664 however, it would mean that COSMO-CLM<sup>2</sup> correctly simulates the mean decrease in H over  
665 forests, but not the associated near surface air warming and increase in LWin. One possible  
666 reason could be that the vertical resolution used (32 vertical levels for the entire atmosphere)  
667 is inadequate, lacking the precision required to simulate these vertical processes in the  
668 shallow NBL. Climate model runs at higher vertical resolution are needed to verify this  
669 hypothesis.

#### 670 **4.4 Difference in daytime SWin**

671 The observed reduction in low and mid-level cloud cover may be a response to a reduction in  
672 turbulence associated with deforestation. Turbulence can cause convective cloud formation in  
673 the boundary layer, especially during summer. However, as shown in the rightmost panel of  
674 Figure 5, the modeled daytime sensible heat flux over open land is significantly lower than  
675 the modeled sensible heat flux over forests, with a mean reduction of about  $50 \text{ Wm}^{-2}$ , which  
676 could definitely contribute to a reduction in cloud cover. No similar consistent decrease in  
677 incoming shortwave radiation during summer days is observed in our FLUXNET site pairs.  
678 However, it is worth noting that this could be related to the specifics of the evaluation setup  
679 used in this study.

680 As mentioned previously, we attempt to simulate the difference in forest and open land  
681 climate observed in FLUXNET site pairs by modifying the land use of a 25 by 25 km model  
682 pixel ( $625 \text{ km}^2$ ). The observational setup, in which we compare flux tower measurements  
683 from two separate real world locations, resembles this situation in land use but not necessarily  
684 in scale. For example, most forest measurement locations are located in relatively small forest  
685 patches ( $2 - 60 \text{ km}^2$ ) surrounded by open land. The forest patches of site pairs DK1, DE1 and  
686 IT2, the 3 site pairs included in the reliable data subset, are approximately  $3 \text{ km}^2$ ,  $60 \text{ km}^2$  and  
687  $10 \text{ km}^2$  in size, respectively. The DK1 and DE1 forest patches are surrounded mostly by  
688 cropland, the IT2 forest patch is surrounded by a mountainous landscape consisting of forests,  
689 grasslands, steep rocky slopes and villages.

690 Therefore, we cannot conclude with any certainty that the decrease in convective uplift and  
691 associated decrease in cloud cover simulated by COSMO-CLM<sup>2</sup> represents a genuine model  
692 bias. Several studies have shown that this mechanism can have a substantial impact when land

693 use is altered on a large scale. For example, in southwestern Australia, a substantial area of  
694 approximately 100,000 km<sup>2</sup> was cleared for agricultural use (mostly wheat) during the 20th  
695 century, while the natural woodlands to the east were left untouched. Observational studies  
696 have shown that the woodlands lower albedo and higher aerodynamic roughness lead to  
697 higher convective activity and a deeper boundary layer. Combined with a local circulation  
698 pattern bringing in moist air from the wheatlands, this resulted in an increase in convective  
699 cloud formation and precipitation (+10%) over the woodlands, and a corresponding decrease  
700 in precipitation over the wheatlands (-30%) [Chambers, 1998]. Land degradation in the Sahel  
701 may have caused a similar shift in local circulation and precipitation, exacerbating the 30 year  
702 drought initially triggered by changes in sea surface temperature in the adjacent Atlantic  
703 Ocean [Foley et al., 2003, Lauwaet et al., 2009, Lauwaet et al., 2010].

704 Therefore, regional climate runs at a higher horizontal resolution (e.g. 1-2 km) are necessary  
705 to determine whether the difference between modeled and observed SWin is in fact caused by  
706 a mismatch in LUC scale. Furthermore, the presence of a scale related bias means the  
707 evaluation methodology presented here is not immediately transferable to GCM's, given the  
708 strong contrast between the scale of LUC represented by our observational site pairs and the  
709 typical resolution currently used for global simulations (100 - 200 km).

## 710 **5 Conclusions**

711 In this study, we present a method for evaluating the impact of LUC on surface climate in  
712 coupled land-atmosphere climate models. The method uses a paired site approach and  
713 differentiates between daytime and nighttime climate. It evaluates both the difference in  
714 surface temperature and the underlying mechanisms by applying a radiative surface  
715 temperature (Ts) change decomposition equation to both observations and model simulations.  
716 We apply it to a state of the art regional climate model used extensively for Europe, namely  
717 COSMO-CLM<sup>2</sup>.

718 Observed differences in 2m air temperature ( $\delta T_a$ ) and radiative surface temperature ( $\delta T_s$ ) for  
719 European open land and forest site pairs are mostly in line with literature reported values for  
720 temperate climate regions, and stress the important contribution of nighttime temperature  
721 change to the daily mean temperature change signal. However, they are not uniformly  
722 reproduced by our climate model. Daytime  $\delta T$  following deforestation is simulated correctly  
723 in winter but underestimated in summer. The impact of deforestation on nighttime Ts, namely  
724 a significant cooling, is not captured in the model. Using the  $\delta T_s$  decomposition equation, we  
725 were able to identify the underlying reasons by determining which LUC related

726 biogeophysical mechanisms were well represented in COSMO-CLM<sup>2</sup>, and which were not  
727 (Table 5).

728 This analysis showed that nighttime cooling is missing from COSMO-CLM<sup>2</sup> mainly because  
729 it does not capture the observed reduction in incident longwave radiation (LWin). We  
730 hypothesize three mechanisms that might be responsible for this reduction in LWin over open  
731 land in the observations: an aerosol effect related to forest VOC emissions, decreased  
732 boundary layer humidity and a reduction in near surface air warming due to increased  
733 nocturnal boundary layer stability. In contrast, two mechanisms responsible for a change in Ts  
734 over open land sites are in fact adequately represented in COSMO-CLM<sup>2</sup>: surface cooling due  
735 to a higher (less negative) sensible heat flux and summertime surface warming due to an  
736 increase in heat storage release. For daytime, one biogeophysical deforestation mechanism in  
737 particular is responsible for the sign and magnitude of observed  $\delta T_s$  values: surface cooling  
738 due to a higher albedo, which is more than compensated by warming due to reduced turbulent  
739 fluxes in summer, but only partly compensated by reduced turbulent fluxes in winter. This  
740 mechanism proved to be reasonably well represented in COSMO-CLM<sup>2</sup>. However, COSMO-  
741 CLM<sup>2</sup> includes an additional atmospheric feedback in summer: the reduction in surface  
742 aerodynamic roughness and associated decrease in turbulent fluxes reduces convective cloud  
743 formation and increases incoming shortwave radiation. There is no evidence for this feedback  
744 in the observational dataset. This might be due to an issue of scale, as the forested vegetation  
745 patches used in the observational dataset (2-60 km<sup>2</sup>) are considerably smaller than the  
746 simulated patches (625 km<sup>2</sup>). Overall, our results highlight the importance of evaluating LUC  
747 effects separately for daytime and nighttime conditions rather than for average conditions.  
748 Averaged values might not reflect reality if the climate model used contains a nighttime bias  
749 similar to what was reported here. To further improve upon the above evaluation, higher  
750 resolution runs (both horizontal and vertical resolution) and more detailed observational data  
751 are needed. Especially for nighttime, detailed vertical profiles of temperature, humidity and  
752 ideally, aerosol concentrations in the nocturnal boundary layer are needed to determine what  
753 mechanisms are responsible for the increase in LWin over forests.

#### 754 **Acknowledgements**

755 The observational datasets used in this manuscript are available for download free of charge  
756 at the European Fluxes Database Cluster (<http://www.europe-fluxdata.eu/>). We thank all site  
757 investigators, their funding agencies and the various regional flux networks (ICOS and  
758 FLUXNET) whose support is essential to the production and distribution of these

759 measurements, without which the model evaluation conducted in this article would not be  
760 possible. SVB was funded by FWO Vlaanderen through the research project DOFOCO. SL  
761 was funded through ERC starting grant 242564. The computational resources and services  
762 used in this work were provided by the VSC (Flemish Supercomputer Center), funded by the  
763 Hercules Foundation and the Flemish Government – department EWI.

764 All authors helped in designing the study. ED created the model code coupling the land  
765 surface and atmospheric model and provided technical support. SVB performed the  
766 simulations and analyzed the data. SVB wrote the manuscript with help from all co-authors.

## 767 **References**

768 Abramowitz, G., R. Leuning, M. Clark, and A. Pitman. 2008. “Evaluating the Performance of  
769 Land Surface Models.” *Journal of Climate* 21 (21): 5468–81. doi:10.1175/2008JCLI2378.1.

770 Akkermans, T., D. Lauwaet, M. Demuzere, G. Vogel, Y. Nouvellon, J. Ardö, B. Caquet, et al.  
771 2012. “Validation and Comparison of Two Soil-Vegetation-Atmosphere Transfer Models for  
772 Tropical Africa.” *Journal of Geophysical Research: Biogeosciences* 117 (G2): G02013.  
773 doi:10.1029/2011JG001802.

774 Akkermans, T., A. Van Rompaey, N. Van Lipzig, P. Moonen, and B. Verbist. 2013.  
775 “Quantifying Successional Land Cover after Clearing of Tropical Rainforest along Forest  
776 Frontiers in the Congo Basin.” *Physical Geography* 34 (6): 417–40.  
777 doi:10.1080/02723646.2013.855698.

778 Akkermans, T., W. Thiery, and N. P. M. Van Lipzig. 2014. “The Regional Climate Impact of  
779 a Realistic Future Deforestation Scenario in the Congo Basin.” *Journal of Climate* 27 (7):  
780 2714–34. doi:10.1175/JCLI-D-13-00361.1.

781 Asharaf, S., and B. Ahrens. 2013. “Soil-Moisture Memory in the Regional Climate Model  
782 COSMO-CLM during the Indian Summer Monsoon Season.” *Journal of Geophysical*  
783 *Research: Atmospheres* 118 (12): 6144–51. doi:10.1002/jgrd.50429.

784 Bala, G., K. Caldeira, M. Wickett, T. J. Phillips, D. B. Lobell, C. Delire, and A. Mirin. 2007.  
785 “Combined Climate and Carbon-Cycle Effects of Large-Scale Deforestation.” *Proceedings of*  
786 *the National Academy of Sciences* 104 (16): 6550–55. doi:10.1073/pnas.0608998104.

787 Baldauf, M., A. Seifert, J. Förstner, D. Majewski, M. Raschendorfer, and T. Reinhardt. 2011.  
788 “Operational Convective-Scale Numerical Weather Prediction with the COSMO Model:

789 Description and Sensitivities.” *Monthly Weather Review* 139 (12): 3887–3905.  
790 doi:10.1175/MWR-D-10-05013.1.

791 Baldocchi, D., and S. Ma. 2013. “How Will Land Use Affect Air Temperature in the Surface  
792 Boundary Layer? Lessons Learned from a Comparative Study on the Energy Balance of an  
793 Oak Savanna and Annual Grassland in California, USA.” *Tellus B* 65 (0).  
794 doi:10.3402/tellusb.v65i0.19994.

795 Bellouin, N., O. Boucher, J. Haywood, and M. Shekar Reddy. 2005. “Global Estimate of  
796 Aerosol Direct Radiative Forcing from Satellite Measurements.” *Nature* 438 (7071): 1138–41.  
797 doi:10.1038/nature04348.

798 Boisier, J. P., N. de Noblet-Ducoudré, and P. Ciais. 2013. “Inferring Past Land Use-Induced  
799 Changes in Surface Albedo from Satellite Observations: A Useful Tool to Evaluate Model  
800 Simulations.” *Biogeosciences* 10 (3): 1501–16. doi:10.5194/bg-10-1501-2013.

801 Boisier, J. P., N. de Noblet-Ducoudré, and P. Ciais. 2014. “Historical Land-Use Induced  
802 Evapotranspiration Changes Estimated from Present-Day Observations and Reconstructed  
803 Land-Cover Maps.” *Hydrol. Earth Syst. Sci. Discuss.* 11 (2): 2045–89. doi:10.5194/hessd-11-  
804 2045-2014.

805 Boisier, J. P., N. de Noblet-Ducoudré, A. J. Pitman, F. T. Cruz, C. Delire, B. J. J. M. van den  
806 Hurk, M. K. van der Molen, C. Müller, and A. Voldoire. 2012. “Attributing the Impacts of  
807 Land-Cover Changes in Temperate Regions on Surface Temperature and Heat Fluxes to  
808 Specific Causes: Results from the First LUCID Set of Simulations.” *Journal of Geophysical  
809 Research: Atmospheres* 117 (D12): D12116. doi:10.1029/2011JD017106.

810 Bonan, G. 2008. “Forests and Climate Change: Forcings, Feedbacks, and the Climate Benefits  
811 of Forests.” *Science* 320 (5882): 1444–49. doi:10.1126/science.1155121.

812 Brovkin, V., M. Claussen, E. Driesschaert, T. Fichefet, D. Kicklighter, M. F. Loutre, H. D.  
813 Matthews, N. Ramankutty, M. Schaeffer, and A. Sokolov. 2006. “Biogeophysical Effects of  
814 Historical Land Cover Changes Simulated by Six Earth System Models of Intermediate  
815 Complexity.” *Climate Dynamics* 26 (6): 587–600. doi:10.1007/s00382-005-0092-6.

816 Carslaw, K. S., O. Boucher, D. V. Spracklen, G. W. Mann, J. G. L. Rae, S. Woodward, and  
817 M. Kulmala. 2010. “A Review of Natural Aerosol Interactions and Feedbacks within the  
818 Earth System.” *Atmos. Chem. Phys.* 10 (4): 1701–37. doi:10.5194/acp-10-1701-2010.

819 Chambers, S. 1998. "Short- and Long-Term Effects of Clearing Native Vegetation for  
820 Agricultural Purposes." PhD. Thesis, University of South Australia, Adelaide, Australia

821 Christy, J.R., W. B. Norris, K. Redmond, and K. P. Gallo. 2006. "Methodology and Results of  
822 Calculating Central California Surface Temperature Trends: Evidence of Human-Induced  
823 Climate Change?" *Journal of Climate* 19 (4): 548–63.

824 Davin, E. L., and N. de Noblet-Ducoudré. 2010. "Climatic Impact of Global-Scale  
825 Deforestation: Radiative versus Nonradiative Processes." *Journal of Climate* 23 (1): 97–112.  
826 doi:10.1175/2009JCLI3102.1.

827 Davin, E. L., R. Stöckli, E.B. Jaeger, S. Levis, and S. I. Seneviratne. 2011. "COSMO-CLM2:  
828 A New Version of the COSMO-CLM Model Coupled to the Community Land Model." *Climate Dynamics* 37 (9-10): 1889–1907. doi:10.1007/s00382-011-1019-z.

830 Davin, E. L., and S. I. Seneviratne. 2012. "Role of Land Surface Processes and Diffuse/direct  
831 Radiation Partitioning in Simulating the European Climate." *Biogeosciences* 9 (5): 1695–  
832 1707. doi:10.5194/bg-9-1695-2012.

833 Demuzere, M., K. Oleson, A. M. Coutts, G. Pigeon, and N. P. M. van Lipzig. 2013.  
834 "Simulating the Surface Energy Balance over Two Contrasting Urban Environments Using  
835 the Community Land Model Urban." *International Journal of Climatology* 33 (15): 3182–  
836 3205. doi:10.1002/joc.3656.

837 De Noblet-Ducoudré, N., J. P. Boisier, A. Pitman, G. B. Bonan, V. Brovkin, F. Cruz, C.  
838 Delire, et al. 2012. "Determining Robust Impacts of Land-Use-Induced Land Cover Changes  
839 on Surface Climate over North America and Eurasia: Results from the First Set of LUCID  
840 Experiments." *Journal of Climate* 25 (9): 3261–81. doi:10.1175/JCLI-D-11-00338.1.

841 Dosio, A., H. J. Panitz, M. Schubert-Frisius, and D. Lüthi. 2014. "Dynamical Downscaling of  
842 CMIP5 Global Circulation Models over CORDEX-Africa with COSMO-CLM: Evaluation  
843 over the Present Climate and Analysis of the Added Value." *Climate Dynamics*, July, 1–25.  
844 doi:10.1007/s00382-014-2262-x.

845 Ehn, M., J. A. Thornton, E. Kleist, M. Sipilä, H. Junninen, I. Pullinen, M. Springer, et al.  
846 2014. "A Large Source of Low-Volatility Secondary Organic Aerosol." *Nature* 506 (7489):  
847 476–79. doi:10.1038/nature13032.

848 Feldmann, H., G. Schädler, H. J. Panitz, and C. Kottmeier. 2013. "Near Future Changes of  
849 Extreme Precipitation over Complex Terrain in Central Europe Derived from High Resolution

850 RCM Ensemble Simulations.” *International Journal of Climatology* 33 (8): 1964–77.  
851 doi:10.1002/joc.3564.

852 Foken, T. 2008. “The Energy Balance Closure Problem: An Overview.” *Ecological*  
853 *Applications* 18 (6): 1351–67. doi:10.1890/06-0922.1.

854 Foley, J. A., M. T. Coe, M. Scheffer, and G. Wang. 2003. “Regime Shifts in the Sahara and  
855 Sahel: Interactions between Ecological and Climatic Systems in Northern Africa.”  
856 *Ecosystems* 6 (6): 524–32. doi:10.1007/s10021-002-0227-0.

857 Hasler, N., D. Werth, and R. Avissar. 2009. “Effects of Tropical Deforestation on Global  
858 Hydroclimate: A Multimodel Ensemble Analysis.” *Journal of Climate* 22 (5): 1124–41.  
859 doi:10.1175/2008JCLI2157.1.

860 Juang, J. Y., G. Katul, M. Siqueira, P. Stoy, and K. Novick. 2007. “Separating the Effects of  
861 Albedo from Eco-Physiological Changes on Surface Temperature along a Successional  
862 Chronosequence in the Southeastern United States.” *Geophysical Research Letters* 34 (21).  
863 <http://cat.inist.fr/?aModele=afficheN&cpsidt=19939784>.

864 Karl, T.R. and Coauthors, 1993: A new perspective on recent global warming: Assymmetric  
865 trends of daily maximum and minimum temperature. *Bull. Amer. Meteor. Soc.*, 74, 1007–  
866 1023

867 Keuler, K., K. Radtke, and G. Georgievski. 2012. Summary of Evaluation Results for  
868 COSMO-CLM Version 4.8\_clm13 (clm17): Comparison of Three Different Configurations  
869 over Europe Driven by ECMWF Reanalysis Data ERA40 for the Period 1979-2000. Cottbus:  
870 Brandenburg University of Technology.

871 Kothe, S., D. Lüthi, and B. Ahrens. 2014. “Analysis of the West African Monsoon System in  
872 the Regional Climate Model COSMO-CLM.” *International Journal of Climatology* 34 (2):  
873 481–93. doi:10.1002/joc.3702.

874 Kotlarski, S., K. Keuler, O. B. Christensen, A. Colette, M. Déqué, A. Gobiet, K. Goergen, et  
875 al. 2014. “Regional Climate Modeling on European Scales: A Joint Standard Evaluation of  
876 the EURO-CORDEX RCM Ensemble.” *Geosci. Model Dev.* 7 (4): 1297–1333.  
877 doi:10.5194/gmd-7-1297-2014.

878 Krinner, G., N. Viovy, N. de Noblet-Ducoudré, J. Ogée, J. Polcher, P. Friedlingstein, P. Ciais,  
879 S. Sitch, and I. C. Prentice. 2005. “A Dynamic Global Vegetation Model for Studies of the

880 Coupled Atmosphere-Biosphere System.” *Global Biogeochemical Cycles* 19 (1): GB1015.  
881 doi:10.1029/2003GB002199.

882 Kurten, T., M. Kulmala, Mi. Dal Maso, T. Suni, A. Reissell, H. Vehkamäki, P. Hari, A.  
883 Laaksonen, Y. Viisanen, and T. Vesala. 2003. “Estimation of Different Forest-Related  
884 Contributions to the Radiative Balance Using Observations in Southern Finland.” *Boreal*  
885 *Environment Research* 8 (4): 275–85.

886 Lauwaet, D., K. De Ridder, and N. P. M. van Lipzig. 2008. “The Influence of Soil and  
887 Vegetation Parameters on Atmospheric Variables Relevant for Convection in the Sahel.”  
888 *Journal of Hydrometeorology* 9 (3): 461–76. doi:10.1175/2007JHM813.1.

889 Lauwaet, D., N. P. M. van Lipzig, and K. De Ridder. 2009. “The Effect of Vegetation  
890 Changes on Precipitation and Mesoscale Convective Systems in the Sahel.” *Climate*  
891 *Dynamics* 33 (4): 521–34. doi:10.1007/s00382-009-0539-2.

892 Lauwaet, D., N. P. M. van Lipzig, N. Kalthoff, and K. De Ridder. 2010. “Impact of  
893 Vegetation Changes on a Mesoscale Convective System in West Africa.” *Meteorology and*  
894 *Atmospheric Physics* 107 (3-4): 109–22. doi:10.1007/s00703-010-0079-7.

895 Lauwaet, D., P. Viaene, E. Brisson, T. van Noije, A. Strunk, S. Van Looy, B. Maiheu, et al.  
896 2013. “Impact of Nesting Resolution Jump on Dynamical Downscaling Ozone Concentrations  
897 over Belgium.” *Atmospheric Environment* 67 (March): 46–52.  
898 doi:10.1016/j.atmosenv.2012.10.034.

899 Lawrence, P. J., and T. N. Chase. 2007. “Representing a New MODIS Consistent Land  
900 Surface in the Community Land Model (CLM 3.0).” *Journal of Geophysical Research* 112  
901 (G1). doi:10.1029/2006JG000168.

902 Lee, X., M. L. Goulden, D. Y. Hollinger, A. Barr, T. A. Black, G. Bohrer, R. Bracho, et al.  
903 2011. “Observed Increase in Local Cooling Effect of Deforestation at Higher Latitudes.”  
904 *Nature* 479 (7373): 384–87. doi:10.1038/nature10588.

905 Lejeune, Q., E. L. Davin, B. P. Guillod, and S. I. Seneviratne. 2014. “Influence of Amazonian  
906 Deforestation on the Future Evolution of Regional Surface Fluxes, Circulation, Surface  
907 Temperature and Precipitation.” *Climate Dynamics*, July, 1–18. doi:10.1007/s00382-014-  
908 2203-8.

909 Luysaert, Sebastiaan, M. Jammet, P. C. Stoy, S. Estel, J. Pongratz, E. Ceschia, G. Churkina,  
910 et al. 2014. “Land Management and Land-Cover Change Have Impacts of Similar Magnitude

911 on Surface Temperature.” *Nature Climate Change* advance online publication (April).  
912 doi:10.1038/nclimate2196.

913 Mahmood, R., R. A. Pielke, K. G. Hubbard, D. Niyogi, P. A. Dirmeyer, C. McAlpine, A. M.  
914 Carleton, et al. 2014. “Land Cover Changes and Their Biogeophysical Effects on Climate:  
915 LAND COVER CHANGES AND THEIR BIOGEOPHYSICAL EFFECTS ON CLIMATE.”  
916 *International Journal of Climatology* 34 (4): 929–53. doi:10.1002/joc.3736.

917 Medvigy, D., R. L. Walko, M. J. Otte, and R. Avissar. 2013. “Simulated Changes in  
918 Northwest U.S. Climate in Response to Amazon Deforestation\*.” *Journal of Climate* 26 (22):  
919 9115–36. doi:10.1175/JCLI-D-12-00775.1.

920 Montes-Helu, M. C., T. Kolb, S. Dore, B. Sullivan, S. C. Hart, G. Koch, and B. A. Hungate.  
921 2009. “Persistent Effects of Fire-Induced Vegetation Change on Energy Partitioning and  
922 Evapotranspiration in Ponderosa Pine Forests.” *Agricultural and Forest Meteorology* 149 (3–  
923 4): 491–500. doi:10.1016/j.agrformet.2008.09.011.

924 Nair, U. S., R. McNider, F. Patadia, S. A. Christopher, and K. Fuller. 2011. “Sensitivity of  
925 Nocturnal Boundary Layer Temperature to Tropospheric Aerosol Surface Radiative Forcing  
926 under Clear-Sky Conditions.” *Journal of Geophysical Research: Atmospheres* 116 (D2):  
927 D02205. doi:10.1029/2010JD014068.

928 Nikulin, G., C. Jones, F. Giorgi, G. Asrar, M. Büchner, R. Cerezo-Mota, O. B. Christensen, et  
929 al. 2012. “Precipitation Climatology in an Ensemble of CORDEX-Africa Regional Climate  
930 Simulations.” *Journal of Climate* 25 (18): 6057–78. doi:10.1175/JCLI-D-11-00375.1.

931 Nogherotto, R., E. Coppola, F. Giorgi, and L. Mariotti. 2013. “Impact of Congo Basin  
932 Deforestation on the African Monsoon.” *Atmospheric Science Letters* 14 (1): 45–51.  
933 doi:10.1002/asl2.416.

934 Oleson, K. W., Y. Dai, G. Bonan, M. Bosilovich, R. Dickinson, P. Dirmeyer, F. Hoffman, P.  
935 Houser, S. Levis, and G. Y. Niu. 2004. Technical Description of the Community Land Model  
936 (CLM). NCAR Technical Note NCAR/TN-461+ STR, National Center for Atmospheric  
937 Research, Boulder, CO.

938 Pitman, A. J., N. de Noblet-Ducoudré, F. T. Cruz, E. L. Davin, G. B. Bonan, V. Brovkin, M.  
939 Claussen, et al. 2009. “Uncertainties in Climate Responses to Past Land Cover Change: First  
940 Results from the LUCID Intercomparison Study.” *Geophysical Research Letters* 36 (14):  
941 L14814. doi:10.1029/2009GL039076.

942 Pitman, A., J., F. B. Avila, G. Abramowitz, Y. P. Wang, S. J. Phipps, and N. de Noblet-  
943 Ducoudré. 2011. "Importance of Background Climate in Determining Impact of Land-Cover  
944 Change on Regional Climate." *Nature Climate Change* 1 (9): 472–75.  
945 doi:10.1038/nclimate1294.

946 Randerson, J. T., H. Liu, M. G. Flanner, S. D. Chambers, Y. Jin, P. G. Hess, G. Pfister, et al.  
947 2006. "The Impact of Boreal Forest Fire on Climate Warming." *Science* 314 (5802): 1130–  
948 32. doi:10.1126/science.1132075.

949 Randow, C. von, A. O. Manzi, B. Kruijt, P. J. de Oliveira, F. B. Zanchi, R. L. Silva, M. G.  
950 Hodnett, et al. 2004. "Comparative Measurements and Seasonal Variations in Energy and  
951 Carbon Exchange over Forest and Pasture in South West Amazonia." *Theoretical and Applied*  
952 *Climatology* 78 (1-3): 5–26. doi:10.1007/s00704-004-0041-z.

953 Ruppert, J., C. Thomas, and T. Foken. 2006. "Scalar Similarity for Relaxed Eddy  
954 Accumulation Methods." *Boundary-Layer Meteorology* 120 (1): 39–63. doi:10.1007/s10546-  
955 005-9043-3.

956 Snyder, P.K., C. Delire, and J.A. Foley. 2004. "Evaluating the Influence of Different  
957 Vegetation Biomes on the Global Climate." *Climate Dynamics* 23 (3-4). doi:10.1007/s00382-  
958 004-0430-0.

959 Spracklen, D. V., B. Bonn, and K. S. Carslaw. 2008. "Boreal Forests, Aerosols and the  
960 Impacts on Clouds and Climate." *Philosophical Transactions of the Royal Society A:*  
961 *Mathematical, Physical and Engineering Sciences* 366 (1885): 4613–26.  
962 doi:10.1098/rsta.2008.0201.

963 Stöckli, R., D. M. Lawrence, G.-Y. Niu, K. W. Oleson, P. E. Thornton, Z.-L. Yang, G. B.  
964 Bonan, A. S. Denning, and S. W. Running. 2008. "Use of FLUXNET in the Community Land  
965 Model Development." *Journal of Geophysical Research* 113 (March): 19 PP.  
966 doi:10.1029/2007JG000562.

967 Takemura, T., T. Nakajima, O. Dubovik, B. N. Holben, and S. Kinne. 2002. "Single-  
968 Scattering Albedo and Radiative Forcing of Various Aerosol Species with a Global Three-  
969 Dimensional Model." *Journal of Climate* 15 (4): 333–52. doi:10.1175/1520-  
970 0442(2002)015<0333:SSAARF>2.0.CO;2.

971 Thiery, W., E. Davin, H. Panitz, M. Demuzere, S. Lhermitte, and N.P.M. Van Lipzig. 2015.  
972 “The Impact of the African Great Lakes on the Regional Climate.” *Journal of Climate*, March.  
973 doi:10.1175/JCLI-D-14-00565.1.

974 Unger, N.. 2014. “Human Land-Use-Driven Reduction of Forest Volatiles Cools Global  
975 Climate.” *Nature Climate Change* 4 (10): 907–10. doi:10.1038/nclimate2347.

976 Van den Hurk, B. JJM, P. Viterbo, A. C. M. Beljaars, and A. K. Betts. 2000. Offline  
977 Validation of the ERA40 Surface Scheme. European Centre for Medium-Range Weather  
978 Forecasts.

979 Vautard, R., A. Gobiet, D. Jacob, M. Belda, A. Colette, M. Déqué, J. Fernández, et al. 2013.  
980 “The Simulation of European Heat Waves from an Ensemble of Regional Climate Models  
981 within the EURO-CORDEX Project.” *Climate Dynamics* 41 (9-10): 2555–75.  
982 doi:10.1007/s00382-013-1714-z.

983 Viterbo, P., and A. C. M. Beljaars. 1995. “An Improved Land Surface Parameterization  
984 Scheme in the ECMWF Model and Its Validation.” *Journal of Climate* 8 (11): 2716–48.  
985 doi:10.1175/1520-0442(1995)008<2716:AILSPP>2.0.CO;2.

986 Vose, R. S., D. R. Easterling, and B. Gleason. 2005. “Maximum and Minimum Temperature  
987 Trends for the Globe: An Update through 2004.” *Geophysical Research Letters* 32 (23):  
988 L23822. doi:10.1029/2005GL024379.

989 Walters, J. T., R. T. McNider, X. Shi, W. B. Norris, and J. R. Christy. 2007. “Positive Surface  
990 Temperature Feedback in the Stable Nocturnal Boundary Layer.” *Geophysical Research*  
991 *Letters* 34 (12): L12709. doi:10.1029/2007GL029505.

992 Werth, D., and R. Avissar. 2002. “The Local and Global Effects of Amazon Deforestation.”  
993 *Journal of Geophysical Research: Atmospheres* 107 (D20): 8087.  
994 doi:10.1029/2001JD000717.

995 Werth, D., and R. Avissar. 2005. “The Local and Global Effects of African Deforestation.”  
996 *Geophysical Research Letters* 32 (12): L12704. doi:10.1029/2005GL022969.

997 Wilson, K., A. Goldstein, E. Falge, M. Aubinet, D. Baldocchi, P. Berbigier, C. Bernhofer, R.  
998 Ceulemans, H. Dolman, and C. Field. 2002. “Energy Balance Closure at FLUXNET Sites.”  
999 *Agricultural and Forest Meteorology* 113 (1): 223–43.

1000 Wouters, H., K. De Ridder, M. Demuzere, D. Lauwaet, and N. P. M. van Lipzig. 2013. “The  
1001 Diurnal Evolution of the Urban Heat Island of Paris: A Model-Based Case Study during

1002 Summer 2006.” *Atmospheric Chemistry and Physics* 13 (17): 8525–41. doi:10.5194/acp-13-  
1003 8525-2013.

1004 Yu, H., S. C. Liu, and R. E. Dickinson. 2002. “Radiative Effects of Aerosols on the Evolution  
1005 of the Atmospheric Boundary Layer.” *Journal of Geophysical Research: Atmospheres* 107  
1006 (D12): AAC 3–1. doi:10.1029/2001JD000754.

1007 Zhang, M., X. Lee, G. Yu, S. Han, H. Wang, J. Yan, Y. Zhang, et al. 2014. “Response of  
1008 Surface Air Temperature to Small-Scale Land Clearing across Latitudes.” *Environmental*  
1009 *Research Letters* 9 (3): 034002. doi:10.1088/1748-9326/9/3/034002.

1010 Zhou, L., R. E. Dickinson, Y. Tian, R. S. Vose, and Y. Dai. 2007. “Impact of Vegetation  
1011 Removal and Soil Aridation on Diurnal Temperature Range in a Semiarid Region:  
1012 Application to the Sahel.” *Proceedings of the National Academy of Sciences* 104 (46):  
1013 17937–42. doi:10.1073/pnas.0700290104.

1014

1015 **Tables**

1016 Table 1: Characteristics of site pairs used in this study.

Cluster name	Lat	Lon	Site name	Elevation (m)	Distance (km)	Data availability	Land use	IGBP class	Climate group
DK1	55,49	11,65	Soroe-LilleBogeskov	40	28,8	2004:2008	Mixed forest	DBF	Temperate
DK1	55,53	12,10	Risbyholm	10	28,8	2004:2008	Cropland	CRO	Temperate
DE1	50,96	13,57	Tharandt	380	8,5	2004:2008	Mixed forest (87% evergreen)	ENF	Temperate
DE1	50,89	13,52	Klingenberg	480	8,5	2004:2008	Cropland	CRO	Temperate
CZ1	49,50	18,54	Bily Kriz Beskidy	908	0,9	2004:2006	Young Norway spruce plantation	ENF	Temperate-Continental
CZ1	49,50	18,54	Bily Kriz Grassland	855	0,9	2004:2006	Grassland (managed as meadow)	GRA	Temperate-Continental
IT2	45,96	11,28	Lavarone	1343	19,3	2003:2008	Mixed coniferous forest	ENF	Temperate
IT2	46,02	11,05	Monte Bondone	1550	19,3	2003:2008	Grassland (managed as meadow)	GRA	Temperate
IT1	41,85	13,59	Collelongo	1550	6,2	2003:2008	Irregularly structured beech forest	DBF	SubTropical-Mediterranean
IT1	41,90	13,61	Amplero	884	6,2	2003:2008	Pasture	GRA	SubTropical-Mediterranean
ES1	39,35	-0,32	El Saler	10	7,8	2004:2006	Pine forest	ENF	SubTropical-Mediterranean
ES1	39,28	-0,32	El Saler-Sueca	41	7,8	2004:2006	Cropland	CRO	SubTropical-Mediterranean
PT1	38,54	-8,00	Mitra Tojal	250	7,4	2004:2005	Cork and holm oak	EBF	SubTropical-Mediterranean
PT1	38,48	-8,02	Mitra Evora	190	7,4	2004:2005	Grassland	GRA	SubTropical-Mediterranean

1017 List of site pairs used in this study, the distance between sites within a pair and the years for  
1018 which common measurements are available. Each site pair is assigned an acronym based on  
1019 its location (e.g. DE1 is located in Germany), and consists of a forest (grey) and an open land  
1020 site (white). In total, 14 sites were used to create 7 site pairs. IGBP classes represented in this  
1021 dataset include deciduous broadleaf forests (DBF), evergreen needleleaf forests (ENF),  
1022 evergreen broadleaf forests (EBF), grasslands (GRA) and croplands (CRO).

1023 Table 2: List of model parameter values for all FLUXNET sites.

<b>Cluster name</b>	<b>Site name</b>	<b>PFT</b>	<b>CTH</b>	<b>LAI<sub>max</sub></b>
<b>DK1</b>	Soroe- LilleBogeskov	BDT-T	20	4,8
<b>DK1</b>	Risbyholm	Crop	0,5	1,4
<b>DE1</b>	Tharandt	NET-T	26,5	7
<b>DE1</b>	Klingenberg	Crop	0,5	2,4
<b>CZ1</b>	Bily Kriz Beskidy	NET-T	12,5	6,7
<b>CZ1</b>	Bily Kriz Grassland	C3 Grass	0,5	2,2
<b>IT2</b>	Lavarone	NET-T	30	8
<b>IT2</b>	Monte Bondone	C3 Grass	0,5	3,2
<b>IT1</b>	Collelongo	BDT-T	21,2	5
<b>IT1</b>	Amplero	C3 Grass	0,5	2,4
<b>ES1</b>	El Saler	NET-T	12	3,1
<b>ES1</b>	El Saler-Sueca	Crop	0,5	1,1
<b>PT1</b>	Mitra Evora	BDT-T	7	2,2
<b>PT1</b>	Mitra Tojal	C3 Grass	0,5	1,7

1024 Shows plant functional type (PFT), canopy top height (CTH) and summer maximum of leaf  
 1025 area index (LAI<sub>max</sub>).

1026 Table 3: Data availability

		1. IT2	2. DE1	3. DK1	4. IT1	5. CZ1	6. PT1	7. ES1	
Number of years		6	5	5	5	3	2	3	
Ta measurements	Entire year	0-24	97	93	96	67	38	70	88
		12-15	97	92	96	67	36	70	88
		0-3	97	92	96	66	35	69	87
	JJA	0-24	93	98	93	83	83	67	100
		12-15	92	97	92	81	78	67	100
		0-3	92	96	91	81	78	67	99
	DJF	0-24	97	85	98	43	0	67	74
		12-15	97	84	98	43	0	67	74
		0-3	96	84	98	42	0	67	74
LWout measurements	Entire year	0-24	96	78	41	17	28	0	0
		12-15	96	77	41	16	27	0	0
		0-3	96	76	40	16	26	0	0
	JJA	0-24	91	75	39	27	55	0	0
		12-15	91	73	38	25	52	0	0
		0-3	91	73	38	26	51	0	0
	DJF	0-24	96	84	42	5	0	0	0
		12-15	95	83	42	5	0	0	0
		0-3	95	81	42	5	0	0	0
Reliable	Entire year	0-24	25	35	21	0	0	0	0
		12-15	6	29	19	0	0	0	0
		0-3	22	41	21	0	0	0	0
	JJA	0-24	24	44	14	0	0	0	0
		12-15	4	36	12	0	0	0	0
		0-3	0	52	15	0	0	0	0
	DJF	0-24	29	34	18	0	0	0	0
		12-15	10	30	17	0	0	0	0
		0-3	49	38	18	0	0	0	0

1027 Data availability for Ta, LWout and reliable decomposition results (see 2.5) in percentage of  
 1028 days with observations. 0-24 denotes the entire day, 12-15 daytime and 0-3 nighttime  
 1029 observations. JJA and DJF were used to distinguish between summer and winter months,  
 1030 respectively. Number of years denotes the number of years for which the sites within a pair  
 1031 have common measurements.

1032 Table 4: Overview of observational studies reporting the effect of deforestation on both  
 1033 surface temperature and all surface energy budget terms.

Study	Location	Temperature variable	Time of Day	dT	Biogeophysical mechanism
Juang 2007	North Carolina	Ts	0-24	+1 K	higher albedo more than offset by reduction in H/LE
			12-15	/	no separate explanation
			0-3	/	no separate explanation
Montes-Helu 2009	Northern Arizona	Ts	0-24	DJF -1 K, JJA +3 to +7K	higher albedo offset by reduction in H/LE, balance depending on season
			12-15	/	no separate explanation
			0-3	/	no separate explanation
Baldocchi 2013	California	potential	0-24	-0.5 K	(DJF) reduction in H (JJA) higher albedo offset by lower LE
		Ta	12-15	DJF -0.8 K, JJA +1.7 K	no separate explanation
			0-3	DJF -0.8 K, JJA -2.2 K	no separate explanation
Lee 2011, Zhang 2014	North America & East Asia, north of 45°N	Ta	0-24	-0.85 K, -0.95 K	separate explanation for day/night
			12-15	0 K, 0 K	higher albedo perfectly offset by reduction in H/LE
			0-3	-2 K, -2 K	reduced turbulence
Lee 2011, Zhang 2014	North America & East Asia, south of 45°N	Ta	0-24	-0.21 K, -0.35 K	separate explanation for day/night
			12-15	+1 K, +1.2 K	higher albedo more than offset by reduction in H/LE
			0-3	-2 K, -1.9 K	reduced turbulence

1034

1035

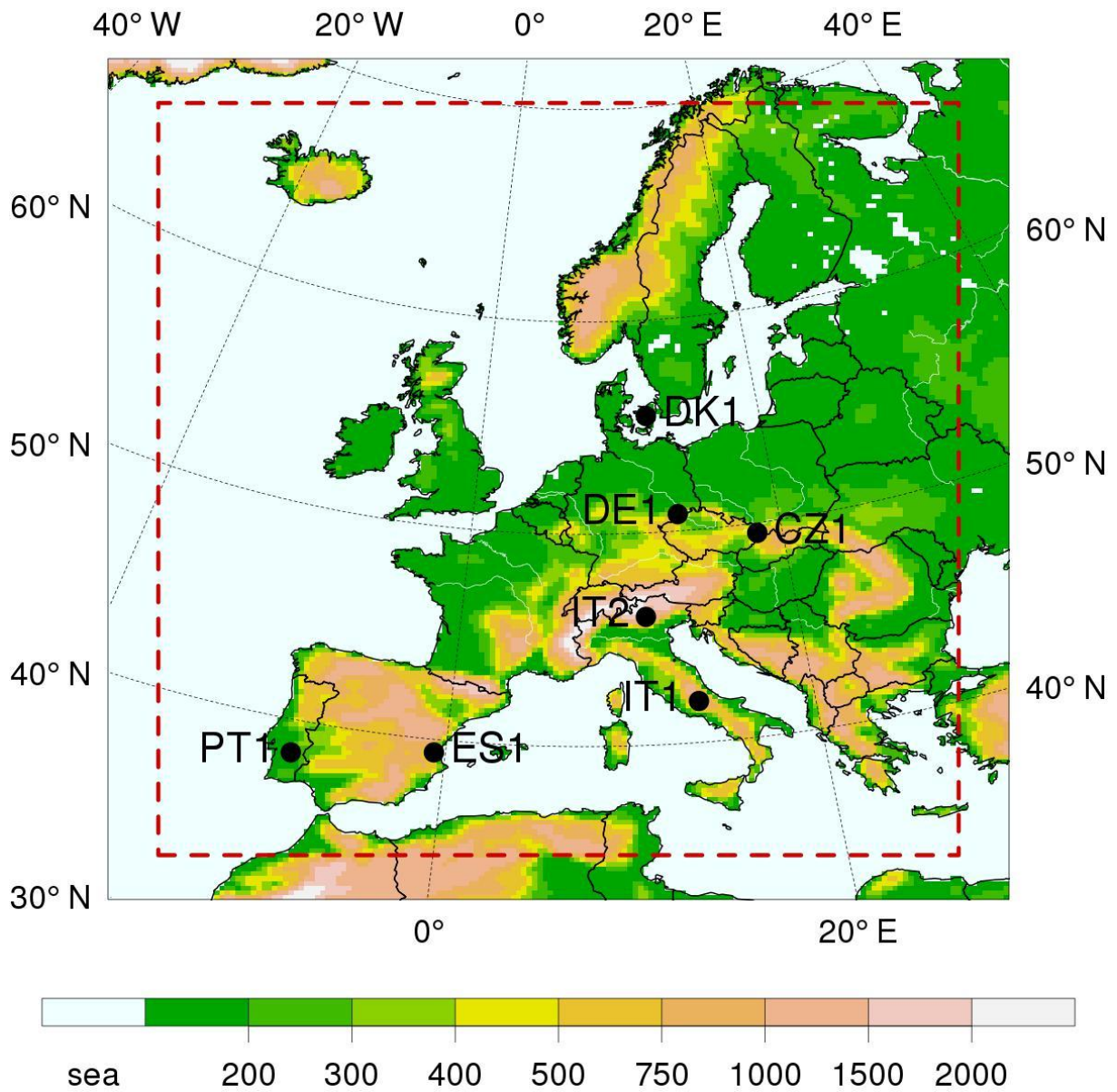
1036 Table 5: Overview of the biogeophysical mechanisms responsible for observed and modeled  
 1037  $\delta T_s$  values.

Effect of deforestation on <b>daytime</b> climate	
<i>Reality</i>	<i>COSMO-CLM<sup>2</sup></i>
Cooling due to lower surface albedo ( <b><math>\alpha_s</math></b> ), which is offset by warming due to reduced surface roughness ( <b><math>R_s</math></b> )	✓
?	Reduced <b><math>R_s</math></b> -> reduced convective uplift -> reduced <b>CLC</b> -> increase in <b>SWin</b> -> surface warming (most prominent in JJA)
Effect of deforestation on <b>nighttime</b> climate	
<i>Reality</i>	<i>COSMO-CLM<sup>2</sup></i>
reduced <b><math>R_s</math></b> -> reduced turbulent mixing -> surface cooling	✓
Lower <b>LWin</b> and associated surface cooling	✗
Surface warming due to more heat storage ( <b>G</b> ) release (JJA)	Surface warming due to more heat storage release ( <b>G</b> ) (JJA & DJF)

1038 Overview of the biogeophysical mechanisms responsible for observed and modeled  $\delta T_s$   
 1039 values. Checkmarks indicate that the mechanism present in reality is included correctly in the  
 1040 model (or vice versa). Question marks indicate that we were not able to determine  
 1041 conclusively if the mechanism included in reality was present in the model (or vice versa).  
 1042 Crosses indicate that the mechanism included in reality was missing from the model (or vice  
 1043 versa).

1044

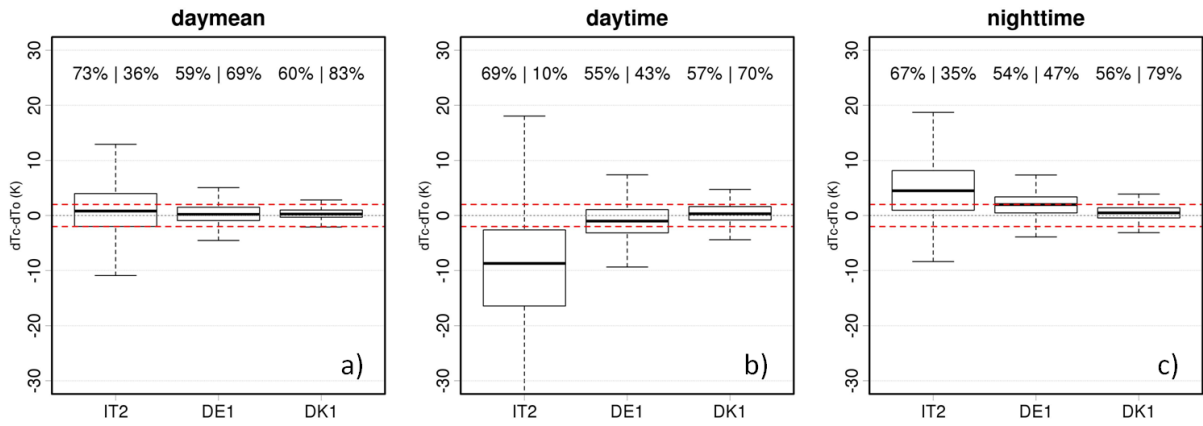
1045 **Figures**



1046

1047 Figure 1: Topography of the model domain and location of the observational pairs. This map  
1048 shows the model domain, including the relaxation zone, the area outside the red rectangle.

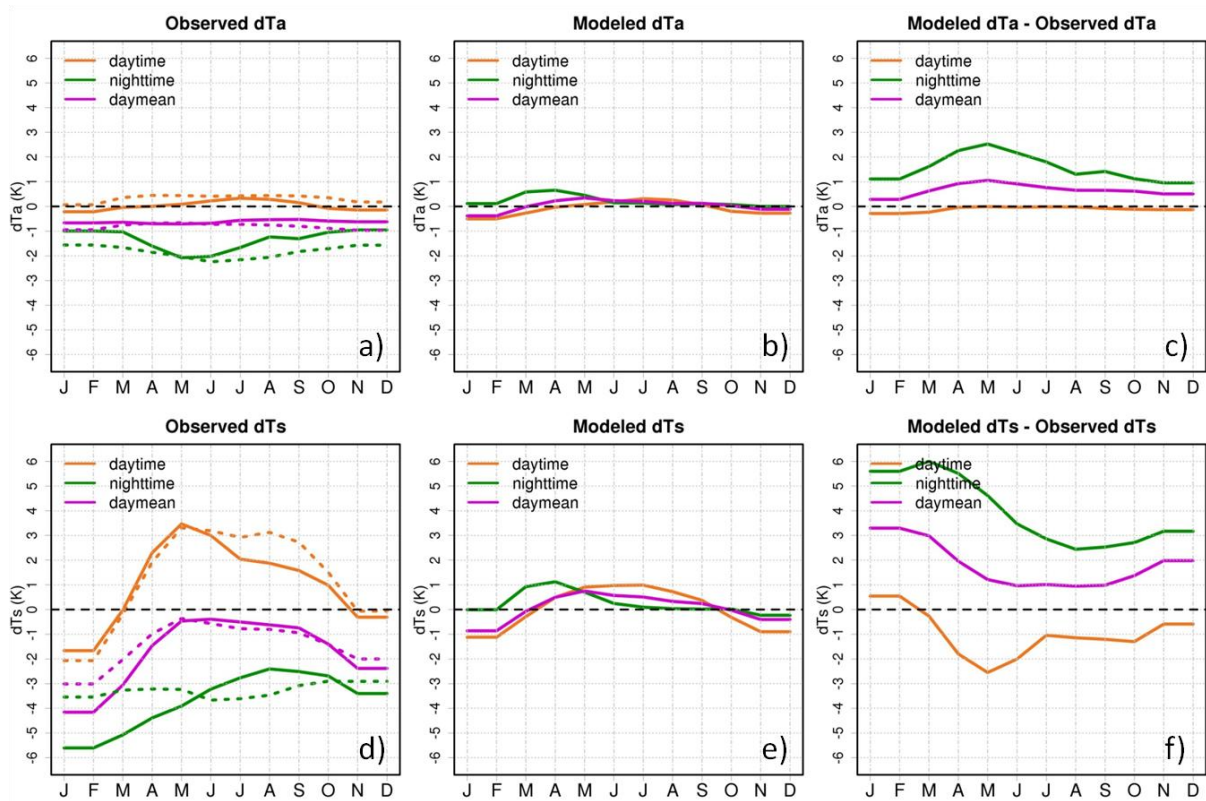
1049



1050

1051 Figure 2: Boxplots of calculated minus observed  $\delta T$ s ( $\delta T_{\text{scal}} - \delta T_{\text{sobs}}$ ). The data reliability  
 1052 range ( $\pm 2\text{K}$ ) is indicated in red. The percentage values printed over the boxplots show two  
 1053 values: the percentage of days with LWout measurements that have measurements for all  
 1054 surface energy budget terms (lefthand value) and the percentage of days with measurements  
 1055 of all surface energy budget terms that are deemed reliable (righthand value).

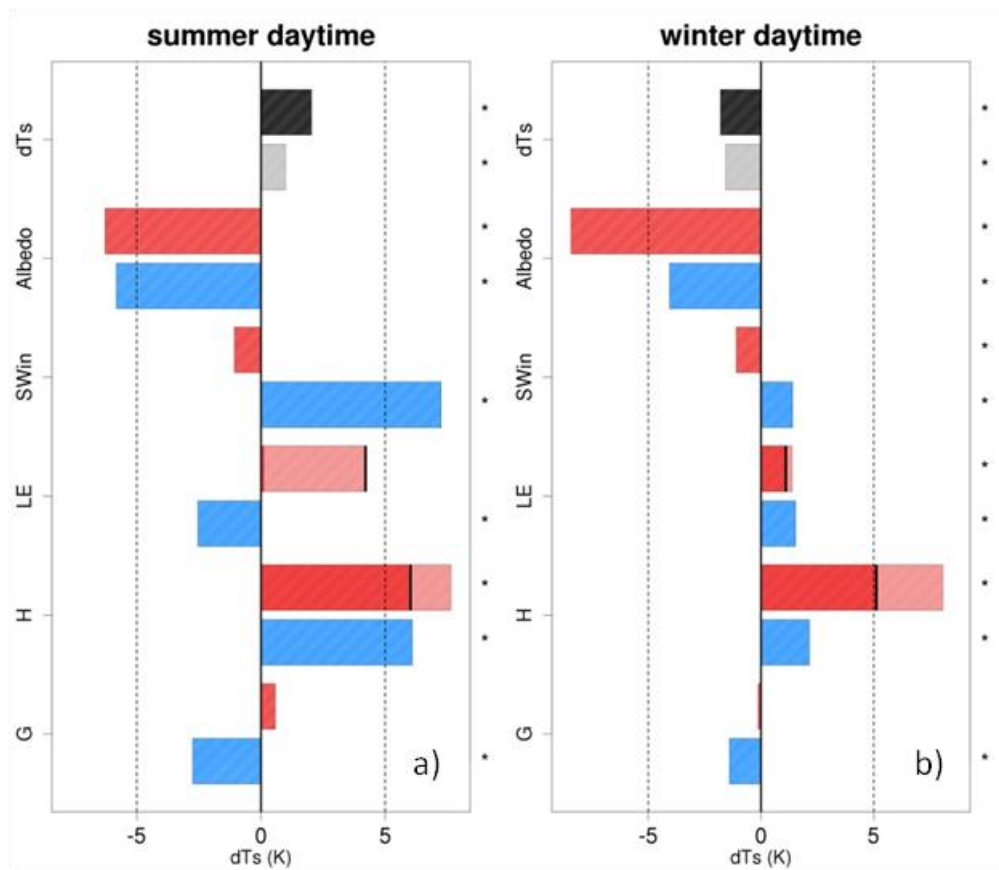
1056



1057

1058 Figure 3: Top row: mean seasonal cycle of a) observed  $\delta T_a$ , b) modeled  $\delta T_a$  and c)  $\delta T_a$  bias  
 1059 (modeled  $\delta T_a$  MINUS observed  $\delta T_a$ ). Bottom row: mean seasonal cycle of d) observed  $\delta T_s$ ,  
 1060 e) modeled  $\delta T_s$  and f)  $\delta T_s$  bias (modeled  $\delta T_s$  MINUS observed  $\delta T_s$ ). For a) and d), the solid  
 1061 lines show the temperature difference for the dataset containing only reliable measurements,  
 1062 while the dashed lines show the temperature difference when all available measurements are  
 1063 used. A 3 month running mean was applied to all timeseries.

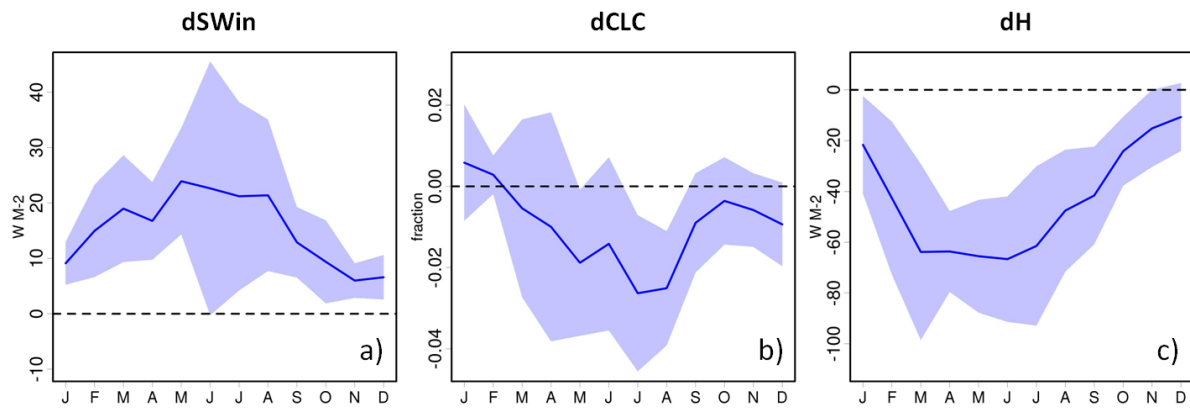
1064



1065

1066 Figure 4: Surface temperature change decomposition for daytime (12-15 UTC), for a) summer  
 1067 and b) winter. All values represent the change associated with deforestation. The modeled and  
 1068 observed mean  $\delta T_s$  is shown on top where black is for the observed values and grey for  
 1069 modeled. The contribution to  $\delta T_s$  for the main components of the surface energy budget are  
 1070 shown in red for observed and blue for modeled values. For sensible and latent heat flux,  $\delta T_s$   
 1071 was calculated using both the original values and the values corrected for surface energy  
 1072 imbalance. The resulting uncertainty is represented by the light colored portion of each bar. A  
 1073 black line indicates the  $\delta T_s$  value calculated with the uncorrected values for H and LE.  $\delta T_s$   
 1074 terms which are significantly different from zero ( $p=0.05$ ) are marked by \*. For reasons of  
 1075 simplicity, components with an associated temperature change that have a yearly mean  
 1076 absolute  $\delta T_s$  value of less than 0.5K across observations and model simulations were not  
 1077 shown. For daytime, this means surface emissivity and incoming longwave radiation.

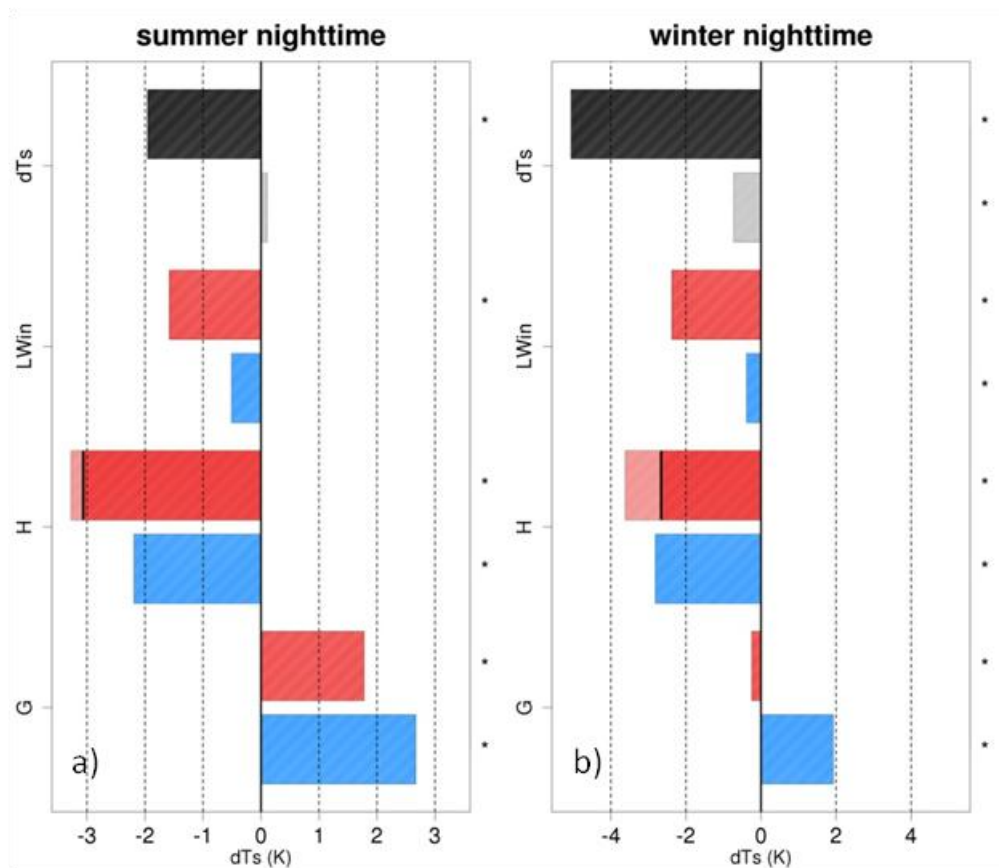
1078



1079

1080 Figure 5: Seasonal cycle of modeled daytime difference for three variables: a) incoming  
 1081 shortwave radiation (SWin), b) low level cloud cover (CLC) and c) sensible heat flux (H).  
 1082 The blue line shows the monthly mean over all 7 site pairs. Also drawn is an area plot of plus  
 1083 and minus one standard deviation. All available data was used for these figures (not just days  
 1084 with reliable observations).

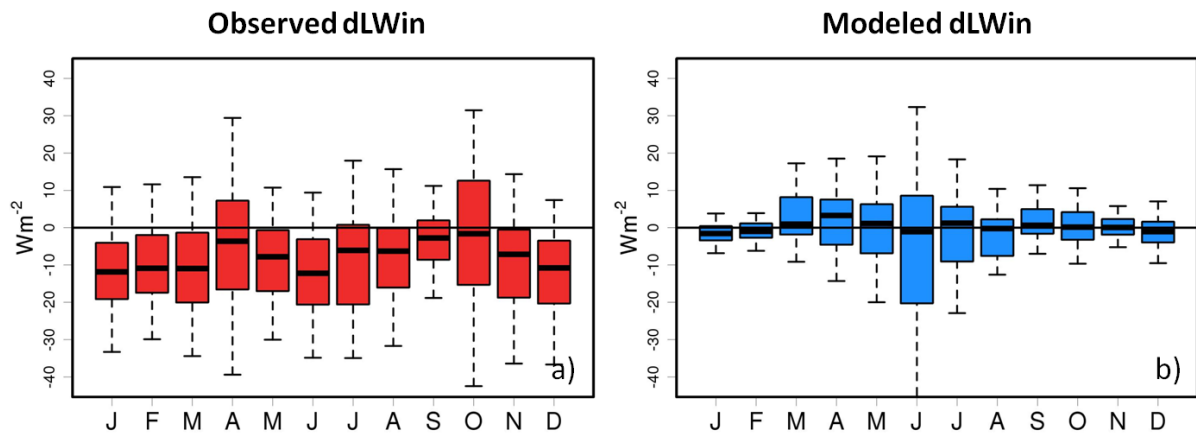
1085



1086

1087 Figure 6: Surface temperature change decomposition for nighttime (00-03 UTC) for a)  
 1088 summer and b) winter. All values represent the change associated with deforestation. The  
 1089 modeled and observed mean  $\delta T_s$  is shown on top where black is for the observed values and  
 1090 grey for modeled. The contribution to  $\delta T_s$  for the main components of the surface energy  
 1091 budget are shown in red for observed and blue for modeled values. For sensible and latent  
 1092 heat flux,  $\delta T_s$  was calculated using both the original values and the values corrected for  
 1093 surface energy imbalance. The resulting uncertainty is represented by the light colored portion  
 1094 of each bar. A black line indicates the  $\delta T_s$  value calculated with the uncorrected values for  $H$   
 1095 and  $LE$ .  $\delta T_s$  terms which are significantly different from zero ( $p = 0.05$ ) are marked by \*. For  
 1096 reasons of simplicity, components with an associated temperature change that have a yearly  
 1097 mean absolute  $\delta T_s$  value of less than 0.5K across observations and model simulations were  
 1098 not shown. For nighttime, this means surface emissivity, incoming shortwave radiation and  
 1099 latent heat flux.

1100

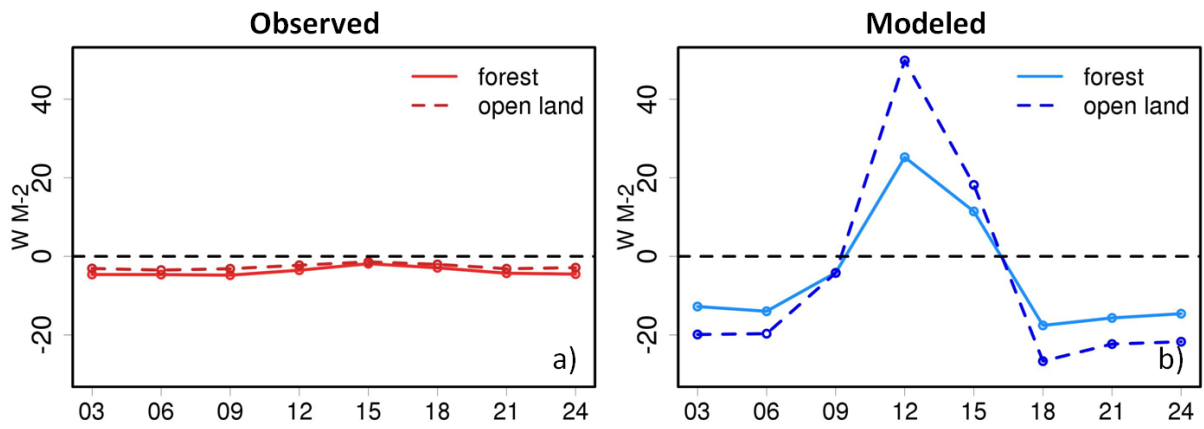


1101

1102 Figure 7: Boxplots of difference in nighttime LWIn (dLWIn) following deforestation for a)  
 1103 observations and b) COSMO-CLM2 model simulations. Only reliable data was used.

1104

### Daily cycle of Ground Flux - Winter



1105

1106 Figure 8: Mean daily cycle of ground flux during winter for a) observations and b) COSMO-  
1107 CLM2 model simulations, for forest and open land sites. Mean over all site pairs. Only  
1108 reliable data was used.